How to cite: *Angew. Chem. Int. Ed.* **2020**, *59*, 10746–10773
International Edition: doi.org/10.1002/anie.201913924
German Edition: doi.org/10.1002/ange.201913924

Single-Molecule Detection

Advances in Optical Single-Molecule Detection: En Route to Supersensitive Bioaffinity Assays

*Zdeněk Farka[+], Matthias J. Mickert[+], Matěj Pastucha, Zuzana Mikušová, Petr Skládal, and Hans H. Gorris**

Keywords:
digital assays · immunoassays · optical detection · signal background · single-molecule detection

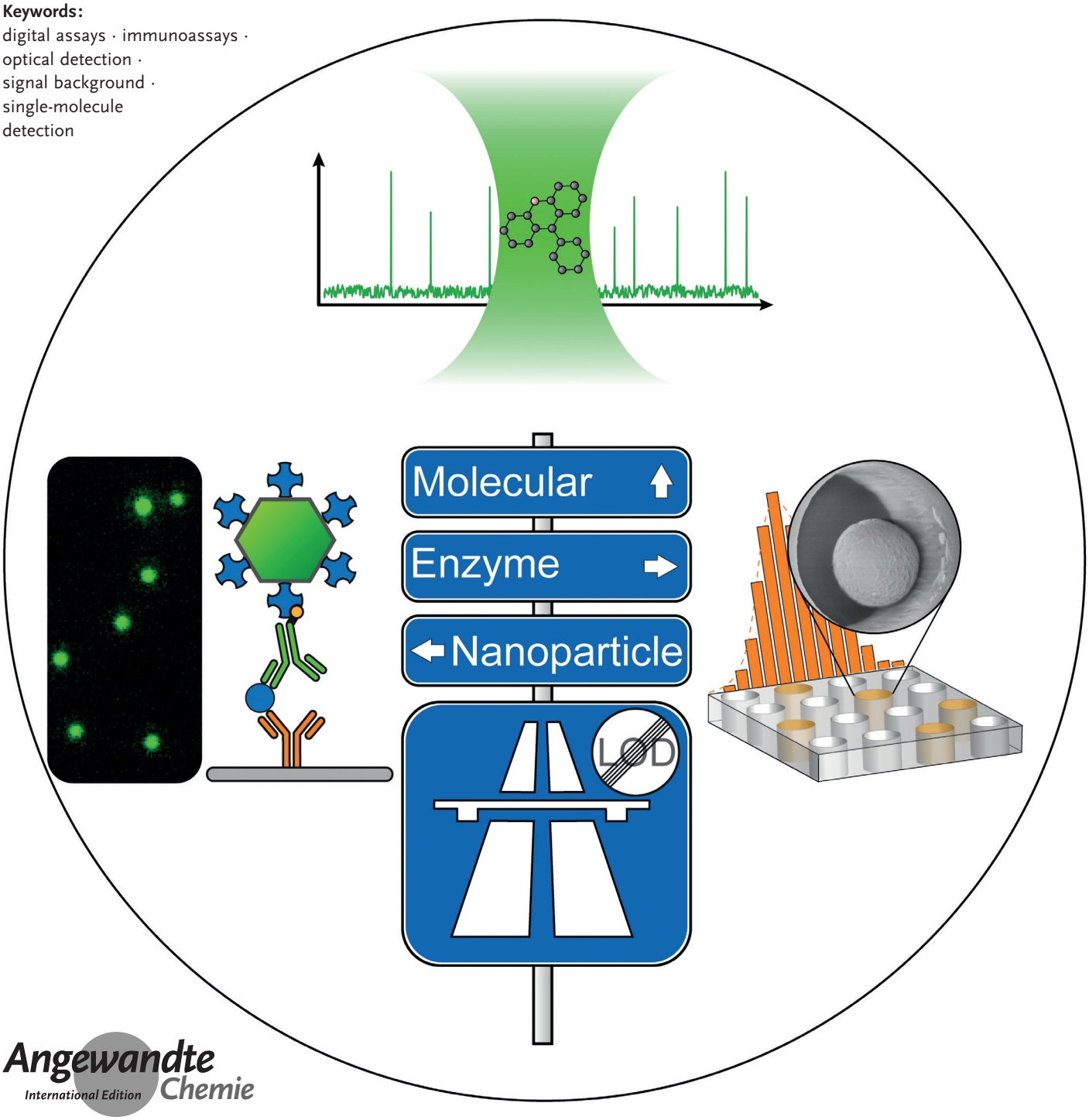

The ability to detect low concentrations of analytes and in particular low-abundance biomarkers is of fundamental importance, e.g., for early-stage disease diagnosis. The prospect of reaching the ultimate limit of detection has driven the development of single-molecule bioaffinity assays. While many review articles have highlighted the potentials of single-molecule technologies for analytical and diagnostic applications, these technologies are not as widespread in real-world applications as one should expect. This Review provides a theoretical background on single-molecule—or better digital—assays to critically assess their potential compared to traditional analog assays. Selected examples from the literature include bioaffinity assays for the detection of biomolecules such as proteins, nucleic acids, and viruses. The structure of the Review highlights the versatility of optical single-molecule labeling techniques, including enzymatic amplification, molecular labels, and innovative nanomaterials.

From the Contents

1. Introduction

The ability to detect individual molecules—at first sight—holds the promise to reach the ultimate sensitivity. Thus, it is not surprising to see a surge in the number and variety of single-molecule approaches. While there have been many review articles on the advantages of single-molecule fluorescence spectroscopy in the field of biophysics,[1] more recent reviews have discussed the potential and limitations of single-molecule applications for analytical chemistry.[2] Our Review is focused on single-molecule bioaffinity assays and does not cover similar techniques for fundamental biophysical or biomolecular research. Furthermore, it was necessary to limit the Review to optical single-molecule techniques. Other emerging single-molecule applications of electrochemical[3] and force-based techniques[4] can be found elsewhere. As the labeling technique is the key element for the ability to detect a single analyte target molecule, the structure of the Review follows different types of optical detection labels. We have also included illustrative examples of label-free optical techniques reported for single-molecule assays.[5]

Most bioaffinity techniques rely on antibodies, though aptamers or molecularly imprinted polymers (MIPs)[6] have also been used to specifically bind and capture an analyte of interest. Antibodies can be generated with high specificity against almost any analyte. Only the affinity ceiling limits their binding constant to approximately $10^{10}\,\text{M}^{-1}$,[7] which is much lower than that of (strept)avidin–biotin binding ($10^{14}\,\text{M}^{-1}$).[8] Since antibodies are rather large, cameloid antibodies that consist only of a single binding site have attracted some attention. The advantage of aptamers is the easy large-scale production, whereas MIPs stand out for their high chemical stability. MIPs are especially useful for the detection of small molecules with a rigid structure. MIPs, however, seem less suitable for the detection of structurally flexible analytes such as proteins.

For detecting the binding event, two approaches can be distinguished: 1) In label-free assays, the binding of the analyte to the detection element results in a signal change that can be directly measured. 2) In the so-called sandwich format, a second affinity reagent, which carries a signal-generating label, binds to the analyte. As a detection label can strongly amplify the signal, this approach is more amenable for implementing single-molecule assays. The first immunoassays used radioactive labels,[9] but enzyme labels have gradually replaced radionuclides for safety reasons and because each enzyme label generates thousands of measurable product molecules (intrinsic signal-amplification step). The enzyme-linked immunosorbent assay (ELISA) is still considered to be the gold standard for the quantitative measurement of various analytes ranging from clinical diagnosis to environmental applications not the least because it is relatively easy to perform.

[*] Dr. Z. Farka,[+] M. Pastucha, Z. Mikušová, Prof. Dr. P. Skládal
CEITEC – Central European Institute of Technology
Masaryk University
625 00 Brno (Czech Republic)
M. J. Mickert,[+] Priv.-Doz. Dr. H. H. Gorris
Institute of Analytical Chemistry, Chemo- and Biosensors
University of Regensburg
Universitätsstraße 31, 93040 Regensburg (Germany)
E-mail: hans-heiner.gorris@ur.de
M. Pastucha, Z. Mikušová, Prof. Dr. P. Skládal
Department of Biochemistry, Faculty of Science
Masaryk University
625 00 Brno (Czech Republic)
[+] These authors contributed equally to this work.
The ORCID identification number(s) for the author(s) of this article can be found under:
https://doi.org/10.1002/anie.201913924.

Over the last 60 years, the development of immunoassays has been mainly driven by making measurements more sensitive, specific, and reproducible. While conventional ELISAs can measure picomolar concentrations of analytes, higher sensitivities are required because even few molecules of toxins can be harmful,[10] individual pathogens can initiate an infectious disease,[11] and trace amounts of a cancer marker indicate the beginning of a malignant transformation.[12] Additionally, the development of more sensitive immunoassays is essential for the discovery of new potential biomarkers that are not accessible using current diagnostic tests.[13]

A conventional ELISA is performed in a laboratory and requires several washing steps and relatively long incubation times. Thus, the second line of immunoassay development has aimed at a faster throughput using lower sample volumes, and assays that can be performed directly at the site of sample collection (on-site testing), for example, at the bedside for diagnostic tests,[14] or in the field for environmental and food products applications. In diagnostics, such assays are commonly known as point-of-care (POC) tests.[15] Minimally invasive sample collection methods, for example, from urine or saliva, and no washing steps are preferred to maintain the user-friendly operation of POC tests. The most famous antibody-based POC test is the home pregnancy test, a very successful example of a lateral flow assay (LFA) first described in the 1980s.[16] The wide acceptance and user-friendliness is a precondition for POC methods to become a cornerstone in the predictive, preventive, personalized, and participatory medicine, commonly termed P4 medicine.[17]

The family of bioaffinity assays, in particular immunoassays, can be subdivided depending on the detection label as shown in Figure 1. 1) Enzyme labels represent the central branch and continue to be the most common detection route. 2) Fluorescent molecular labels are in principle easier to implement because the detection antibody is directly labeled with a fluorophore and no enzymatic amplification step is necessary. The simplest form, the fluorescence immunoassay (FIA), however, is limited by background fluorescence without the advantage of enzymatic amplification. In addition to the direct intensity-based fluorescence detection, this scheme was adapted for signal amplification (e.g. by Immuno PCR) or for the development of homogeneous assays using fluorescence polarization. Nevertheless, the non-zero background of fluorescence remains. A decisive breakthrough was the development of time-resolved (TR) detection by employing lanthanide-based labels that display a long lifetime (microseconds) compared to organic fluorophores (nanoseconds).[18] In a time-gated approach, after luminescence excitation, the signal acquisition is delayed by a few microseconds to let the autofluorescence signal decay, and only the specific signal of the lanthanide is recorded. The TR-FIA is a background-free optical detection method that, however, requires a more sophisticated instrumental setup. The dissociation-enhanced lanthanide fluorescent immunoassay (DELFIA) is the most prominent TR-FIA system on the market.[19]

Nanoparticles (NP) currently constitute the most rapidly branching labeling strategy for immunoassays.[20] Colloidal gold has been used for the readout of LFAs. Due to their plasmonic properties, gold nanoparticles (Au NPs) strongly absorb and scatter light such that a direct color read-out by eye is possible, and the user is able to make a yes/no decision. In the meantime, the use of NPs in immuno- and other bioaffinity assays has experienced a fast growth as a result of concurrent progress in nanomaterials research. Plasmonic NPs are now in widespread use, but also other NPs and nanocomposites have been designed that enable a convenient optical readout. For example, quantum dots (QDs) are

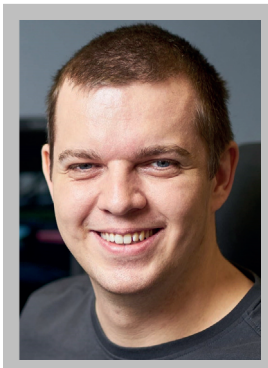

Zdeněk Farka received his PhD in structural biology in 2017 under the supervision of Petr Skládal at the Central European Institute of Technology (CEITEC), Masaryk University (Brno, Czech Republic). He completed research internships at the University of Regensburg (Germany) with Hans-Heiner Gorris and at the University of Rouen (France) with Niko Hildebrandt. He is currently working as a Senior Researcher at CEITEC. His research interests include the detection of proteins and bacteria via various immunoanalytical techniques.

Matěj Pastucha is a PhD student of biochemistry at Masaryk University. He received a Master's degree in analytical biochemistry in 2015 and is currently pursuing his PhD under the supervision of Petr Skládal. His research focuses on the development of immunochemical assays and sensors for the detection of proteins and bacteria. This includes antibody immobilization to diverse substrates, their conjugation with nanoparticles or other labels, and detection utilizing optical or electrochemical readout.

Matthias J. Mickert is a PhD student at the Institute of Analytical Chemistry, Chemo- and Biosensors of the University of Regensburg in the group of Hans-Heiner Gorris. His research interests include single-molecule enzyme kinetics in femtoliter arrays and the development of digital immunoassays using photon-upconversion nanoparticles as background-free luminescent labels. He is specialized in the surface modification, characterization, and imaging of upconversion nanoparticles.

Zuzana Mikušová graduated with a degree in biotechnology at the Slovak University of Technology in Bratislava in 2014. She is now a PhD student under the supervision of Petr Skládal at Masaryk University. She is currently focusing on immunosensing in the electrochemistry field as well as the immunocytochemistry of cells, both using nanoparticles as labels.

a better alternative to organic fluorophores because they are more photostable and brighter, which is an important feature for single-molecule applications. Photon-upconversion nanoparticles (UCNPs) are another emerging class of labels that can be excited by near-infrared light and emit shorter-wavelength light. The anti-Stokes emission prevents autofluorescence and light scattering and thus allows for an optical readout without background interference.[21] The background-free detection renders UCNPs an excellent candidate for single-molecule applications.[22] Furthermore, nanocontainers such as liposomes can be filled with large numbers of fluorophores to generate a strong signal. In contrast to enzyme labels that generate the fluorophores in situ, the encapsulated fluorophores are released on demand from the nanocontainer to avoid self-quenching inside the confined environment.[23] There are also mixed detection schemes, e.g., in the form of electrochemiluminescence that generates a strong signal without background.

All three branches shown in Figure 1 have now blossomed into single-molecule assays as a consequence of innovative assay designs as well as advances in instrumental techniques, detector sensitivities and data processing capabilities. In simple terms, single-molecule assays can be considered as the result of driving conventional assays to the highest sensitivity—either by increasing the specific signal to very high levels or by background reduction. Therefore, any standard analytical method can, in principle, reach "single-molecule sensitivity" but background interference such as matrix effects, readout noise or non-specific binding typically prevents it.

It is furthermore essential to understand that the ability to detect a single molecule is not synonymous with the most sensitive analytical assay. For example, some immunoassays from the pre-single-molecule era actually had higher sensitivities than current single-molecule assays.[24] If we shift our attention from the detection of a single molecule as the "ultimate" sensitivity to the distinct readout mode, however, it becomes clear that single-molecule detection is a unique and powerful tool for background reduction. Since the signal of a single detection label can be reliably distinguished from the background noise of the instrument and reagents, the measurement is completely independent of background fluctuations. Thus, the term "digital assay" (as opposed to a conventional "analog assay") is a much better description of the advantages conferred by single-molecule detection in analytical chemistry. The digital readout, in turn, makes the measurement more robust and thus indirectly leads to lower detection limits.

The signal-to-noise (S/N) ratio determines whether a single molecule can be detected or not. The strength of the specific optical signal depends on the type of label and can be strongly amplified, as discussed in the next section. In a digital assay, however, each detectable response is derived from a single analyte molecule, and thus the specific signal strength is ultimately fixed. The only option to assure single-molecule detection is the reduction of the background signal, which decreases with the detection volume. This problem has been extensively discussed for fluorescence spectroscopy, one of the earliest and most important methods for single-molecule detection, but similar considerations also hold for nonfluorescent single-molecule detection methods. Fluorescent molecules are capable of generating a strong signal because each fluorophore can emit up to a million photons before it finally photobleaches. Fluorescence excitation, however, also leads to an optical background signal due to autofluorescence and light scattering.[25] In order to observe a single fluorescent molecule, it is essential to reduce the detection volume to a femtoliter (fL) volume—commonly by using confocal microscopy, fluorescence correlation spectroscopy (FCS), or total internal reflection microscopy (TIRF).

The requirement for a very small detection volume is associated with two closely related problems that must be addressed in order to achieve higher sensitivity with digital assays. The first problem is analyte sampling. At very low analyte concentrations, there are not enough molecules present in an analyte sample to reach the detection volume by diffusion on a reasonable timescale. For example, it was estimated that it takes on average more than ten minutes for a molecule present in a concentration of 1 fM to reach a detection volume of 10 fL by diffusion.[26] Stochastic fluctuations are the second problem.[27] At low analyte concentrations, a small observation volume is randomly at one time occupied by a single analyte molecule and, at another time, empty. The so-called Poisson noise ($(\sqrt{n})/n$) depends on the number of counted events (n) and is negligible in conventional analog assays where n is very large. For digital assays, however, it presents a problem because a single detection event of an analyte molecule does not contain enough analytical information. Therefore, it is necessary to make either many parallel measurements on a larger area or many sequential measurements in the same detection volume.

Petr Skládal is an Associate Professor and Head of the Department of Biochemistry, Faculty of Science, Masaryk University. He received his PhD in the field of amperometric biosensors in 1992. After research stays (1991, 1993) at the University of Florence (Italy) with Marco Mascini, he continued to investigate biosensors at Masaryk University. He currently also heads the Nanobiotechnology Research Group at CEITEC. His research interests include enzymatic and immunochemical biosensors using electrochemical and piezoelectric transducers.

Hans-Heiner Gorris studied biology at the University of Münster (Germany) and obtained his PhD degree from the University of Lübeck (Germany). After working on single-molecule enzyme assays with David Walt at Tufts University (USA), he joined the Institute of Analytical Chemistry, Chemo- and Biosensors at the University of Regensburg (Germany) in 2009. He has been a Heisenberg-Fellow of the DFG since 2016. His research interests include background-free luminescent bioaffinity assays based on UCNPs with single-molecule sensitivity as well as new methods for investigating enzyme kinetics at the single-molecule level.

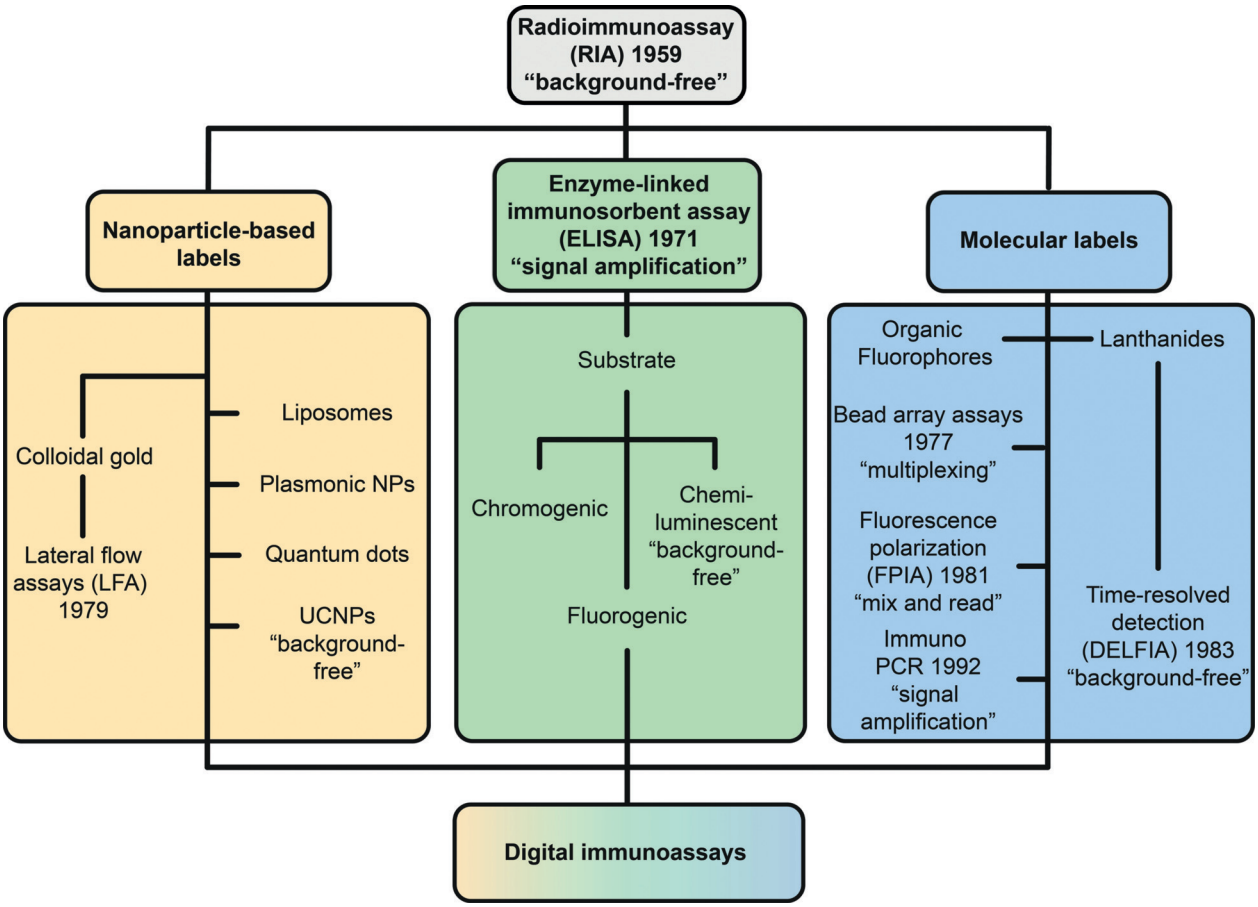

Figure 1. Progress in the development of immunoassays using optical detection schemes towards single-molecule detection. Radioisotopes were replaced by labels based on enzymes, fluorescent molecules, and nanoparticles. Through the choice of an appropriate readout method, all these labels can be exploited for measurement at the single-molecule level.

2. Enzyme Labels

ELISA has been successfully transformed into single-molecule immunoassays. The generation of thousands of fluorescent molecules per enzyme label molecule multiplied by up to a million photons per fluorophore generates a very strong signal that can be detected by simple wide-field fluorescence microscopy. In particular, β-galactosidase from *Escherichia coli* is an excellent enzyme label for single-molecule applications because it is robust and can turn over up to 1000 substrate molecules per second. Based on this strategy, Rotman[28] reported the very first single-molecule experiment already in 1961. The enzymatic substrate turnover, however, is a kinetic process and requires time, which leads to product diffusion. Consequently, the signal is not detectable at the same location as the analyte. There are two options to spatially allocate the signal to the analyte.

2.1. Assays Based on Localized Product Deposition

In the easiest case, the enzymatic reaction generates a product that precipitates around the analyte. The group of Suzuki[29] designed a digital sandwich immunoassay on beads by using a conjugate of detection antibody and horseradish peroxidase. The enzyme label converted a fluorescence-labeled tyramide substrate to a short-lived radical which immediately coupled the fluorescent labels only to the analyte-bearing beads. This led to a high local fluorescence signal at the site of analyte binding. It was noted, however, that the detection of the tyramide signal on the beads by flow cytometry was less efficient than that of digital ELISAs in confined environments.

2.2. Assays in Confined Environments

Alternatively, the enzyme label converts a substrate to a soluble fluorescent product. In this case, the reaction must be confined in a very small compartment in order to prevent product diffusion.[30] The concentration of the reaction product exceeds the detection threshold in small confined volumes. For example, a single molecule of β-galactosidase enclosed in a volume of 50 fL (50 μm^3) can produce a fluorophore concentration of 2 μM in 1 min, which can be easily detected via conventional epifluorescence microscopy.[31] Enzymatic reactions were confined in water-in-oil emulsion[28] or microfluidic droplets, fused silica capillaries,[32] virus

capsids,[33] lipid vesicles,[34] or so-called femtoliter arrays. In particular, femtoliter arrays and water-in-oil microfluidic droplets have found analytical applications.

2.2.1. Femtoliter Arrays

Femtoliter arrays consist of a large number of homogeneous wells fabricated in the surface of optical fiber bundles,[35] fused silica slides,[36] or polydimethylsiloxane (PDMS).[37] The Walt group[38] pioneered single-molecule immunoassays based on a fluorogenic enzymatic reaction in femtoliter arrays, which was commercialized by Quanterix. In the so-called Simoa platform (single-molecule arrays, Figure 2), magnetic beads with a capture antibody were dispersed in a sample. The bead concentration was typically much higher than the analyte concentration. The beads were magnetically separated and incubated with a biotinylated antibody, followed by the addition of a streptavidin–β-galactosidase conjugate. A high bead-to-analyte ratio resulted in a small fraction of beads labeled with a single enzyme molecule and a large excess of unlabeled beads. The beads were loaded with a fluorogenic substrate onto a femtoliter array and sealed with a gasket or oil film. A highly fluorescent product accumulated only in wells that contained a bead with a bound analyte molecule. The analyte concentration was determined digitally by counting the number of fluorescent wells. Prostate-specific antigen (PSA) and tumor necrosis factor-α (TNF-α) were detected with a limit of detection (LOD) of 1.5 fg mL^{-1} (≈50 aM) and 2.5 fg mL^{-1} (≈150 aM), respectively. Other clinically relevant analytes included cancer biomarkers,[39] urinary biomarkers,[40] p24 protein of HIV,[41] and the neurofilament light chain protein (NFL), a neuronal injury marker of various neurodegenerative conditions and brain injuries. Traditionally, cerebrospinal fluid must be obtained for analysis by lumbar puncture because the concentration of NFL in the blood is too low for a conventional ELISA. Shahim et al.[42] developed an ultrasensitive immunoassay with an LOD of 0.29 pg mL^{-1}, which enabled NFL measurements in the serum of healthy subjects. Olivera et al.[43] determined tau protein in blood plasma (LOD of 0.012 pg mL^{-1}) to examine the relationship between increased tau protein levels and chronical neurological and psychological symptoms in military personnel after a traumatic brain injury. The ultrasensitive detection of biothreats such as ricin has also been demonstrated.[44]

The Noji group[45] developed larger arrays of one million femtoliter wells. Counting a very high number of individual immunocomplexes in the arrays reduced the Poisson noise. The assay was employed for the detection of PSA with an LOD of 60 ag mL^{-1} (≈2 aM). The authors also showed that the digital assay in femtoliter arrays is amenable to multiplexing by using two different enzyme/substrate labels.[46] Recently, a competitive femtoliter array format was demonstrated for the detection of small molecules such as cortisol in saliva.[47] The assay achieved an IC_{50} down to 0.42 ng mL^{-1}, which was 44 times lower than for a conventional ELISA.

2.2.2. Microdroplets

Different methods for the generation of water-in-oil microdroplets have been reviewed earlier.[30] Water-in-oil droplets enclose the reactants and the product into pico- to femtoliter volumes. While microdroplets generated by emulsification methods tend to be rather heterogeneous, more homogeneous microdroplets can be generated and handled by microfluidic devices. Microfluidic droplets separate the reactants from the liquid substances, reduce the assay volume, and enable rapid handling, which increases the assay throughput.[48] Microfluidic droplets have also been used to study single enzyme molecule reactions[49] and single cells.[50]

Water-in-oil femtoliter droplets generated by a microfluidic device were used to establish a bead-based ELISA (Figure 3).[51] A capture antibody on the surface of polystyrene beads immobilized PSA. The presence of PSA was then detected by a biotinylated detection antibody and a streptavidin–β-galactosidase conjugate using fluorescein-di-β-D-galactopyranoside (FDG) as the substrate. The enzyme product fluorescein was recorded by fluorescence microscopy while the beads were identified and counted based on their red autofluor-

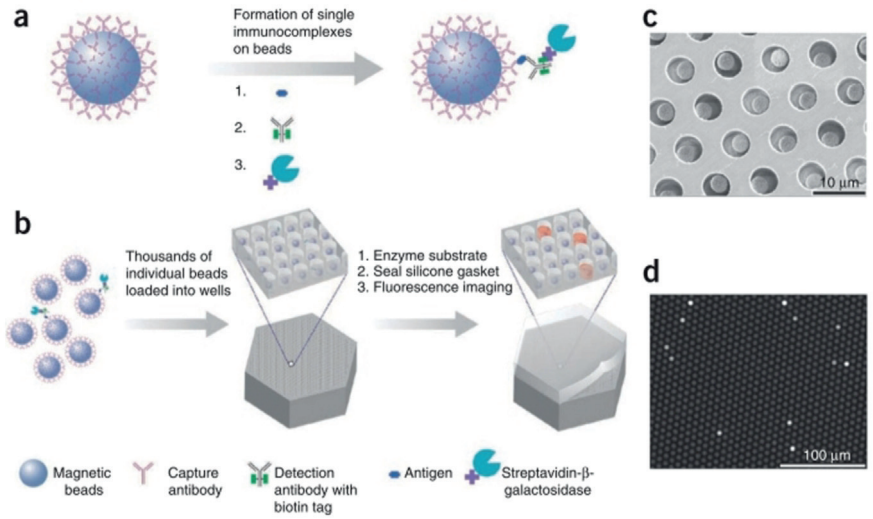

Figure 2. Single-molecule ELISA assay in femtoliter arrays. a) Many magnetic beads coated with capture antibody are dispersed in the analyte sample. After an analyte molecule has been caught, a biotinylated antibody forms the sandwich complex and serves as an anchor for a streptavidin-modified β-galactosidase. b) The beads are loaded—together with a fluorogenic substrate—onto a femtoliter array and sealed by a PDMS gasket. c) Scanning electron microscopy shows that only one bead is loaded per femtoliter well. d) Fluorescence microscopy records the fluorescence increase in wells that contain a bead with a captured analyte molecule. Reprinted with permission from ref. [38]. Copyright 2010 Nature America.

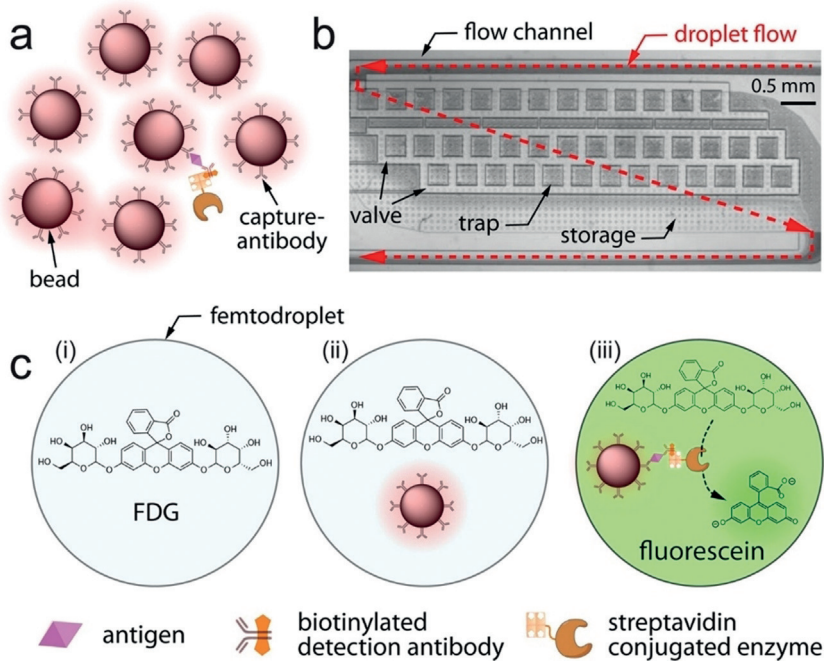

Figure 3. Scheme of single-molecule immunoassay in femtoliter-sized droplets. a) Antibody–antigen complex formation on beads. b) Beads with or without immunocomplex are encapsulated in droplets with the substrate and incubated on chip in traps to collect the fluorescent products of single-enzyme labels. c) Three droplet populations can be distinguished: i) droplets without a bead, ii) those containing a bead without immunocomplex, and iii) those containing both a bead and immunocomplex, which exhibit a positive fluorescence signal due to the enzymatic activity of a single β-galactosidase label. Reprinted with permission from ref. [51]. Copyright 2013 American Chemical Society.

escence. The microdroplet assay achieved an LOD of 46 fM and a linear range of 0.046–4.62 pM.

Liu et al.[52] developed another type of enzyme-linked immunoassay on magnetic beads for single-exosome counting in microdroplets (droplet digital ExoELISA). Magnetic beads were equipped with an anti-CD63 antibody to capture exosomes. After sample incubation, a biotinylated detection antibody and a streptavidin–β-galactosidase conjugate were added to the beads. The beads were enclosed in 40 μm droplets (≈33 fL) containing FDG. The fluorescence increase of fluorescein was detected in each droplet containing a magnetic bead with captured exosome. A bead-to-droplet ratio of 0.3 was employed to ensure that only one magnetic bead was enclosed in a given droplet. The assay achieved an LOD down to 10 enzyme-labeled exosome complexes per microliter (≈10 aM).

An competitive bead-based immunoassay utilizing microdroplets was reported for the detection of α-fetal protein (AFP).[53] AFP was captured by antibody-coated magnetic beads followed by the addition of a biotinylated detection antibody and a streptavidin–β-galactosidase conjugate. After magnetic separation, the unbound streptavidin–β-galactosidase was injected into a microfluidic chip to generate microdroplets with FDG. The microdroplets were collected into a microtiter plate and fluorescent droplets containing free streptavidin–β-galactosidase were counted under a fluorescence microscope. This indirect digital concentration readout reached an LOD in the fM concentration range.

The Di Carlo group[54] developed a microfluidic digital homogeneous entropy-driven biomolecular assay (dHEBA) for the detection of influenza A. Upon nucleoprotein binding, nucleic acid labeled antibodies formed a catalytically active complex that drove a hybridization/displacement reaction on a multicomponent nucleic acid substrate and generated many fluorescence-labeled oligonucleotides. The dHEBA format enabled the detection of influenza A nucleoprotein in a concentration of 4 aM in approximately 10 min without the need for a purification step.

3. DNA Labels for PCR Amplification

The polymerase chain reaction (PCR) amplifies DNA—in principle starting from a single template strand—exponentially to very high copy numbers of DNA.[55] Droplet microfluidics on a microchip enables the rapid isolation of single DNA strands and subsequent PCR amplification in pico- or femtoliter reaction containers.[56] For example, a digital PCR was performed in rotational chips to detect viral RNA isolated from single HIV viruses.[57] Wells of different volumes were employed in the chip to enable quantification over a wider dynamic range. The assay achieved an LOD of 40 RNA molecules per mL.

Similar to the digital readout of single enzyme molecule labels, a digital immuno-PCR can be implemented if the PCR reaction is enclosed in microdroplets. The droplet-based digital immuno-PCR (ddIPCR) used magnetic beads as a solid support, DNA as a marker and PCR for signal amplification, for example, for the detection of PSA.[58] The ddIPCR was performed in three steps as shown in Figure 4. First, the PCR reaction mixture was emulsified to generate tens of thousands of water-in-oil droplets per microchip. Subsequently, the samples underwent thermal amplification cycles and the number of positive droplets was determined by end-point fluorescence detection. In the last step, the number of DNA copies was calculated based on the Poisson distribution. The ddIPCR can usually improve the LOD by 100- to 10000-fold compared to a standard ELISA. It was noted, however, that the washing steps and the microfluidic droplet system cannot be easily combined. The LOD for PSA was 0.48 $ng\,mL^{-1}$ with a linear range of 0.5–30 $ng\,mL^{-1}$. The concentration analysis of human serum samples correlated well with a commercial reference immunoassay.

The digital PCR was combined with a proximity ligation assay (PLA) to improve the precision of the assay.[59] Target proteins such as the cytokine IL-6 were immobilized on magnetic beads and detected by two types of DNA-modified antibodies that are capable of forming a pair of PLA probes. If both antibodies bound to the protein, the PLA probes were

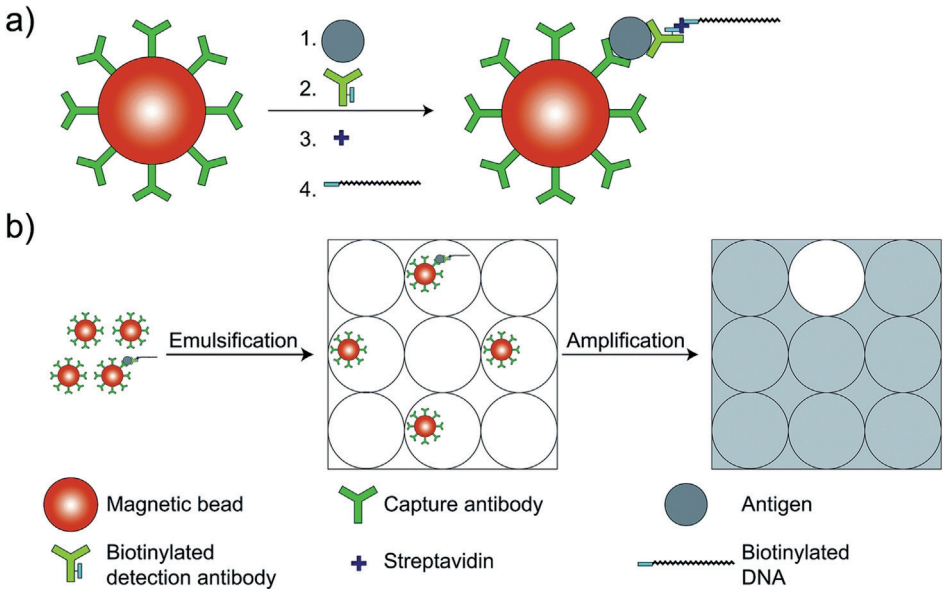

Figure 4. Scheme of ddIPCR. a) Antibody-coated magnetic beads capture the antigen (1). A biotinylated antibody (2), streptavidin (3), and biotinylated DNA sequence from *Aspergillus fumigatus* (4) are sequentially added. b) The magnetic beads are resuspended in a reaction mixture and emulsified. After ddIPCR, the numbers of negative and positive droplets are counted. Reprinted with permission from ref. [58]. Copyright 2018 Royal Society of Chemistry.

joined by DNA ligation. The ligated DNA reporter strand was then amplified by rolling circle amplification, and the amplified DNA was detected via fluorescent DNA probes. Because standard rolling circle amplification is not quantitative, the ligated DNA strands were compartmentalized individually by using a microfluidic device, and the protein concentration was determined digitally by counting fluorescent microdroplets.

4. Fluorescent Molecular Labels

The detection of molecular labels at the single-molecule level relies on fluorescence spectroscopy and microscopy. Confocal microscopy and total internal reflection microscopy (TIRF) efficiently reduce the detection volume and the concomitant background signal, which enables the detection of single fluorescent label molecules. When crossing a focused laser beam in a confocal microscope set-up, individual fluorophores emit bursts of photons that are detected.[60] The residence time depends on the diffusion of the fluorophore through the beam path (with a typical active volume of a few femtoliters) and on photobleaching. Cyanine dyes were proposed for such applications as the excitation within 650–700 nm is well compatible with the spectral window of low light scattering and autofluorescence of biological substances including blood. Even epifluorescence has more recently been reported to enable single-fluorophore detection. However, the type of microscopy is not relevant for the assay design as long as it allows for the detection of a single fluorescent molecule. Thus, we have organized this section according to different assay formats. Fluorescence counting of single protein analyte molecules immobilized on a surface by capture antibodies seems in general to be more sensitive than correlation techniques in solution.

4.1. Detection of Surface-Bound Analytes

Löscher et al.[61] developed a sandwich assay for the detection of single cardiac actin molecules. The scanning system employed a single-photon-counting avalanche photodiode together with a CCD camera for imaging under 635-nm laser excitation. A glass surface was coated with a cellulose layer to reduce nonspecific binding. Confocal microscopy reduced the optical background by minimizing the detection volume, which enabled the evaluation of photon bursts originating from individual molecules.

A particular kind of bioaffinity assay, the so-called pull-down assay, has been used for the identification of protein–protein interactions. The Ha group[62] developed a single-molecule pull-down assay (Figure 5). A capture antibody was immobilized in a flow chamber coated with polyethylene glycol (PEG) and biotin. Streptavidin was added to the flow chamber, followed by the addition of a biotinylated anti-His antibody, which captured overexpressed His6-tagged yellow fluorescent protein (YFP) from cell extracts. Individual YFP molecules were detected by TIRF microscopy. A stepwise decrease of the fluorescence intensity during single-molecule bleaching experiments enabled the identification of dimeric and trimeric YFP molecules. Individual protein kinase A (PKA) complexes were detected by a two-color single-molecule pull-down assay. In its inactive form, PKA is present as a tetramer that consists of two catalytic and two regulatory subunits. Cyclic adenosine monophosphate (cAMP) activates the enzyme and leads to tetramer dissociation. The investigation of the stoichiometry of individual PKA complexes is essentially not possible using conventional analog detection.

Burgin et al.[64] developed a single-molecule assay for the detection of enhanced green fluorescent protein (EGFP) and tumor suppressor protein p53. A microfluidic chip was mounted onto a TIRF microscope under 473-nm laser excitation. Two methods for absolute protein quantification were used for the digital readout. In the accumulation method (Figure 6a), the analyte was observed over a defined time period, during which the number of fluorescent spots increased until individual EGFP molecules were no longer distinguishable as diffraction-limited spots. In the detect and bleach method (Figure 6b), fluorescent spots were counted, bleached, and after a fixed time interval counted again. Both images were subtracted to identify newly arrived and

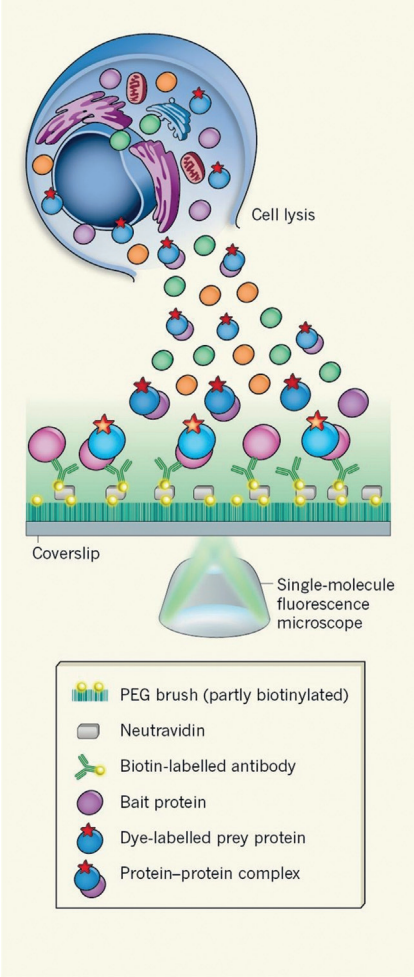

Figure 5. Scheme of single-molecule pull-down assay. A cell lysate is applied directly onto a coverslip for single-molecule TIRF microscopy. Specific antibodies on the coverslip capture protein complexes. Prey proteins associated with the bait protein are detected via a fluorescent dye fused to the prey. Reprinted with permission from ref. [63]. Copyright 2011 Macmillan Publishers Limited.

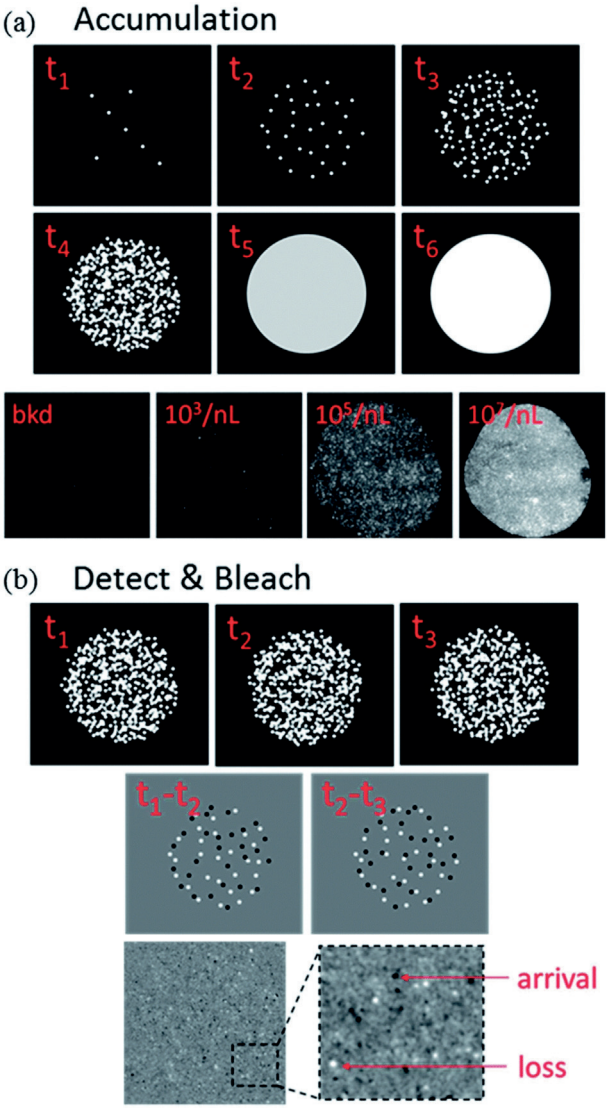

Figure 6. Different approaches for digital protein quantification. a) For low analyte concentrations, the accumulation method counts the increasing number of fluorescent spots. If the distance between two fluorescent molecules is below the diffraction limit, they appear as one spot and cannot be distinguished anymore. b) In the detect and bleach method, fluorescent molecules are counted after a certain time interval and subsequently bleached. The bleaching step keeps the average number of fluorophores bound to the surface at a constant level such that higher concentrations can be determined. Reprinted with permission from ref. [64]. Copyright 2014 Royal Society of Chemistry.

bleached molecules. Protein p53 was detected in the accumulation method by using a labeled detection antibody.

Zhang et al.[65] developed a digital ATP assay using split aptamers. A coverslip was bound to a glass slide with a 5-mm hole in the center, followed by surface activation with plasma. A mixture of poly(L-lysine)-poly(ethylene glycol)-biotin (PLL-PEG-biotin) and PLL-PEG was added to the activated coverslip. Next, streptavidin was added, and a biotinylated Cy3-3′-labeled split aptamer was bound to streptavidin. The analyte ATP was added together with the other Cy5-3′-labeled aptamer. The coverslip was placed on an epifluorescence microscope, and the emission of the two dyes was collected simultaneously on the same EM-CCD camera. Diffraction-limited spots of a mixed color indicated specific binding, whereas spots with only one color indicated nonspecific binding. The assay achieved an LOD of 100 fM and a working range of 1 pM to 5 nM.

Weng et al.[66] developed an aptasensor for the detection of small molecules. The hairpin-shaped aptamer immobilized on a glass slide changes its conformation to an open state upon analyte binding (Figure 7). Fluorescently labeled short ssDNA probes bound preferably (but not exclusively) to the open conformation and the fluorescence trajectories of individual aptamers were monitored by TIRF microscopy. As the binding of the fluorescent probe followed different kinetic patterns depending on the conformation of the aptamer, the kinetic fingerprints were used to distinguish between nonspecific binding and analyte binding. Only spots that showed the signature of specific binding were counted to determine the analyte concentration. The assay achieved

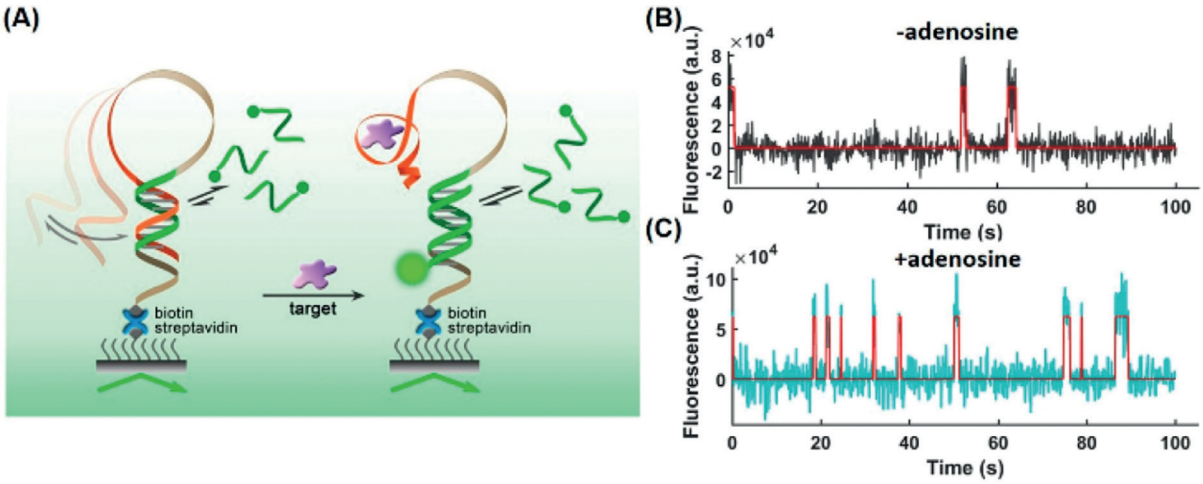

Figure 7. A) Scheme of a hairpin-shaped aptasensor immobilized on a slide surface. Analyte binding results in a conformational change and binding of a complementary fluorescent ssDNA probe. Single-molecule trajectories B) without and C) with 50 pM adenosine are distinguishable. Reprinted with permission from ref. [66]. Copyright 2019 American Chemical Society.

LODs of 0.3 pM for adenosine, 0.35 pM for acetamiprid, and 0.72 pM for PCB-77 in spiked chicken meat extract.

4.2. Laser-Induced Fluorescence Detection inside a Capillary

The Yeung group pioneered the use of capillary electrophoresis for single-molecule detection.[36] In capillary electrophoresis, an electric field drives the sample through the illumination volume, which is small enough to allow for the detection of individual fluorescent molecules. Based on the electrophoretic mobility of individual fluorescently labeled antibodies, fluorescent immunoassays were established.[67] Antibodies bound to an analyte molecule have lower electrophoretic mobility and can thus be distinguished from free antibodies using cross-correlation. Individual fluorescence-labeled antibodies were recorded in the capillary by wide-field microscopy using a 20× objective (numerical aperture (NA) 0.75) and an intensified CCD camera.

Stimulated by the need for reliable and sensitive assays for cardiac troponin, a diagnostic marker of acute myocardial infarction, the Erenna platform was developed.[68] First, a sandwich immunoassay was performed in a microtiter plate, and the bound labels were then released and inserted into a capillary electrophoresis device. As only a single fluorescent molecule passed through the detection volume during the observation interval, individual analyte molecules were counted, and an LOD of 1.7 pg mL^{-1} was achieved. In combination with magnetic beads, it was possible to detect troponin I levels of 0.2 pg mL^{-1}, which are typically found in healthy individuals (0.3 to 9 pg mL^{-1}).[69] Esparza et al.[70] used the Erenna assay to study amyloid-beta (Aβ) aggregation and deposition in Alzheimer's disease. Concentrations as low as 1.56 pg mL^{-1} (0.18 pM) of soluble Aβ oligomers were detectable above background, and the limit of quantification (LOQ) was 6.25 pg mL^{-1} (0.72 pM). The method was applied to measure the Aβ oligomers in human cortical tissue homogenate. Wild et al.[71] detected mutant huntingtin protein (mHTT) in cerebrospinal fluid. The mHTT is a promising biomarker for monitoring Huntington disease progression, but due to its predominantly intracellular localization, the concentration in the cerebrospinal fluid is very low (below pM even in patients in an advanced state of the disease) and conventional methods are not sensitive enough to detect it. The Erenna assay provided an LOD of 40 fM and the authors found a significant difference in levels of mHTT in carriers of the genetic mutation in the premanifest stage and in different later stages of the disease.

For the detection of the fertility-related human gonadotropin follicle-stimulating hormone (FSH), the laser beam was shaped into stripes, and 10 "superpixel" zones were evaluated using a CCD camera.[72] Magnetic beads served as a solid support for the immunoassay. The LOD for FSH was 34 fM for a few hundreds of fluorescent events counted above the background in 12 s corresponding to a few zeptomoles of labeled antibodies.

The combination of several excitation lasers (blue 488 nm; green 543 nm; red 635 nm; infrared 730 nm) and four single-photon-counting modules allowed for the implementation of multiplexed assays.[73] Confocal microsecond-scale alternating-laser excitation (ALEX) single-molecule fluorescence spectroscopy was used to probe the fluorescent acceptor (A) without energy transfer (FRET) and provided donor (D) excitation-based data for each single molecule. Distinct emission signatures were recovered for interacting species through determination of the FRET efficiency E, which relates to the D–A distance, and distance-independent stoichiometry-based ratio S. The combination of E and S on two-dimensional histograms allowed for a virtual sorting of single molecules. This technique was evaluated by determining 25 DNA sequences, 6 tumor markers, 8 bacterial gene markers, and 3 drug-resistance determinants.

4.3. Fluorescence Correlation Spectroscopy

Fluorescence correlation spectroscopy (FCS) records diffusion at the single-molecule level. Equilibrium concentration fluctuations due to Brownian motion are measured as spikes of fluorescence intensity within a small sampling volume. A concentration in the nanomolar range should be attained for sub-femtoliter detection volumes to allow for following individual fluorescence-labeled molecules. Such a small detection volume can be obtained using confocal microscopy or multiphoton microscopy. The sensitivity of FCS depends mainly on the brightness of the fluorescent probe and on the detection volume.[74] Evaluating fluorescence intensity fluctuations over time by an autocorrelation function yields information on the diffusion rates and the concentration of the fluorescent molecule.[75] The diffusion time depends on the size and shape of the target molecule, on the viscosity of the solution, and on the size of the focused laser beam. FCS can be exploited to follow molecular interactions with other molecules because the diffusion time decreases each time when another molecule has bound.[76] FCS has found applications in in vitro and in vivo studies of protein–protein interactions, nucleic acid interactions, enzymatic activities, and membrane diffusion.[77]

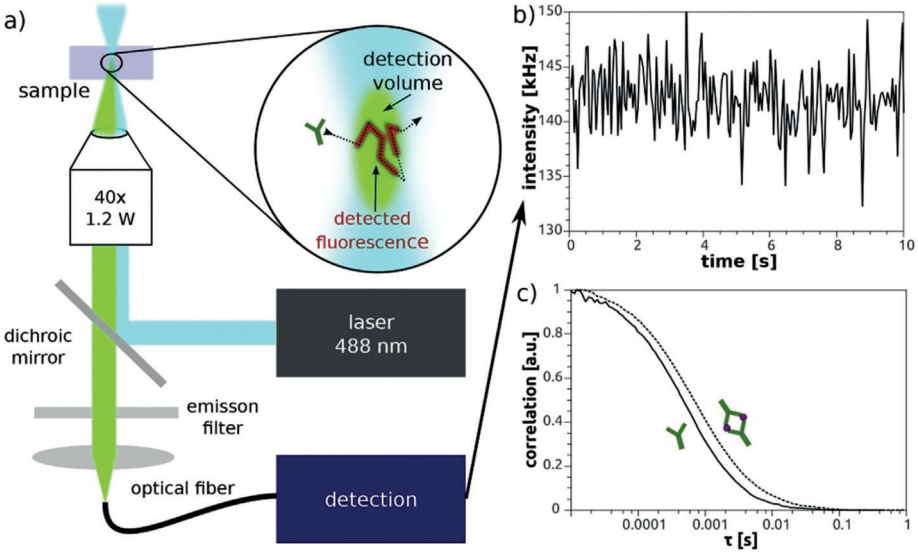

Figure 8. a) FCS setup. A laser is focused to excite fluorescent molecules in a confocal volume. Fluorescence intensity fluctuations due to Brownian motion are measured in solution by a photodiode connected to an optical fiber. b) The emitted photons are collected and plotted as time-dependent intensity changes. c) The autocorrelation curves show an increase in the diffusion time after formation of the immunocomplex (•••••) compared to the antibody alone (——). Reprinted with permission from ref. [76]. Copyright 2017 Elsevier.

The detection of fluorescence-labeled molecules at the single-molecule level by FCS is applicable for the implementation of homogeneous immunoassays that avoid washing and separation steps as well as nonspecific binding to surfaces, which becomes increasingly important at low analyte concentrations.[75] On the other hand, FCS is prone to background interferences caused by autofluorescence, light scattering, quenching, and potential aggregation of the assay components. The simplest scheme of an FCS immunoassay is based on following the changes in the diffusion rate after the formation of the immunocomplex (Figure 8). Chatterjee et al.[76] employed a sandwich assay for the detection of the neuronal cell adhesion molecule contactin-2 in cerebrospinal fluid. The assay was based on two different anti-contactin antibodies. One antibody was labeled with Alexa Fluor 488 and the other one was unlabeled. The formation of the sandwich immunocomplex of both antibodies with the analyte increased the diffusion time, which was evaluated from the autocorrelation curve. The authors reached a limit of quantification of 0.2 ng mL^{-1}.

Changes in the diffusion rates were also recorded by FCS to implement a competitive assay for the detection of the mycotoxin fumonisin B_1 (FB_1).[78] The analyte FB_1 competed with a tracer consisting of FB_1 and Alexa Fluor 488 for the free binding site of the antibody. The assay provided an LOD of 1 ng mL^{-1}.

The sensitivity towards the formation of immunocomplexes closer in size can be enhanced by using fluorescence cross-correlation spectroscopy (FCCS). FCCS uses two spectrally different fluorescent probes, which can be simultaneously excited using two separate excitation wavelengths and detected in two different channels. The amplitudes of the cross-correlation curves are calculated to measure the interactions of the fluorescent probes with the analyte. Compared to conventional FCS, the use of two labels increases the sensitivity and especially the selectivity of FCCS in the quantitative measurement of biomolecules.

The Klenerman group[79] developed a sandwich assay based on the counting of coincidence spikes of two labeled antibodies. Compared to conventional FCCS, the data evaluation was simplified because only the number of spikes was counted, which corresponds to both labels being present in the confocal volume at the same time. Protein G and herpes simplex virus were detected with an LOD of 50 fM.

Miller et al.[80] demonstrated a sandwich FCCS-based assay for the detection of human chorionic gonadotropin and the prion protein (Figure 9). Two lasers were alternated, and the emissions of different fluorescent labels were measured using separate detectors to eliminate spectral cross-talk and reduce the probability of false positive cross-correlation.[81] The fluorophores were chosen in such a way that their emission is separated, reducing the overlap of the emission and the possible energy transfer. To eliminate aggregation effects on the cross-correlation curves, cross-correlations on short time sections were calculated and those displaying the highest level of fluorescence (top 1% of the intensity distribution) were discarded. The method provided

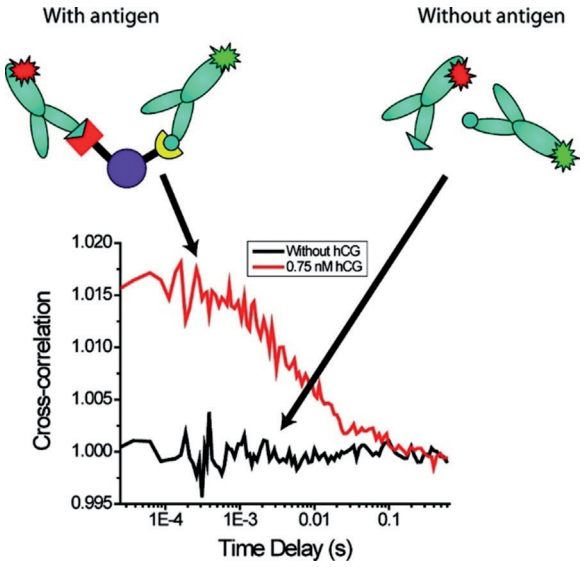

Figure 9. In FCCS, two fluorescence-labeled antibodies bind to the analyte. Black line: cross-correlation of labeled antibodies without analyte (antigen); red line: cross-correlation of labeled antibodies in the presence of the analyte. Reprinted with permission from ref. [80]. Copyright 2009 American Chemical Society.

LODs of 100 pM (human chorionic gonadotropin) and 2 nM (prion protein) with an analysis time of 40 min.

5. Nanoparticle Labels

In recent years, various kinds of nanomaterials have been introduced as labels for immunoassays in order to enhance the assay performance.[20a] In particular, NPs with luminescent or plasmonic properties, which allow for a convenient optical readout, are suitable for single-molecule analysis.[82] Compared to molecular labels, NPs display generally higher signals, which allows for an easier readout. On the other hand, their larger size can be a drawback in terms of steric hindrance of the immunocomplex formation as well as a potentially higher degree of nonspecific binding.

5.1. Semiconductor Nanoparticles

Quantum dots (QDs) are fluorescent semiconductor nanocrystals with dimensions typically between 1 and 10 nm. The photoluminescence properties of QDs can be tuned by changing the nanocrystal size, making it possible to adjust emission wavelengths in the range of 380 to 2000 nm.[83] Compared to conventional fluorophores, QDs provide higher emission intensities, better photostability, wider excitation spectra, and narrower emission bandwidths.[84] This allows for an easier detection of individual QDs compared to conventional fluorophores.

5.1.1. Detection of Surface-Bound Analytes

Liu et al.[85] developed a sandwich immunoassay based on QD labels. Capture antibody-coated QDs and detection antibody-coated QDs were mixed with the sample, and then immobilized onto a positively charged coverslip. Mixed color spots (yellow) were counted under a fluorescence microscope. Carcinoembryonic antigen (CEA) was detected with an LOD of 6.1 pM. The same group[86] implemented a homogeneous sandwich immunoassay that employed only one type of label. Capture and detection antibodies were conjugated separately to 655QD. After formation of a sandwich immunocomplex with the analyte, the QD emission was monitored through a diffraction grating placed in front of a CMOS camera of the microscope. The grating divided the emission into a zeroth-order spot and a first-order streak. Because of the diffraction limit, it was not possible to distinguish between unbound QDs and the immunocomplexes. The QDs were oxidized during excitation, and the first order streak shifted to shorter wavelengths. The oxidation of the QDs started at different times and proceeded at different rates, which split the first order streak into two smaller streaks. The number of split streaks was proportional to the number of analyte molecules. The LODs for CEA and AFP were 6.7 fM and 3.4 fM, respectively.

5.1.2. Detection in Microchannels

The Nie group[87] implemented a sandwich immunoassay for virus detection based on the parallel detection of red and green fluorescent NPs in a microfluidic channel under 488-nm laser excitation. The immunocomplex was detected by monitoring the coincidence of photon bursts in the red and green detection channels. In this way, wild-type and mutated respiratory syncytial viruses were quantified in parallel with an LOD of 4×10^6 plaque-forming units (PFU).

Zhang et al.[88] developed an aptamer-based single-QD FRET assay for the detection of cocaine. They first designed a signal-off assay by assembling a sandwich of a 3′-biotinylated oligonucleotide, a cocaine aptamer and a 3′-Cy5-labeled oligonucleotide. The sensitivity of the system was investigated by plotting the Cy5 burst counts against the ratio of Cy5 to 605QD from 0 to 24. It was possible to distinguish between single Cy5 labels. The sandwich complex was dispersed in a diluted cocaine sample to capture the analyte, and then a commercial streptavidin-functionalized 605QD (605 nm emission) was added to capture the aptamer complex. In the presence of a high amount of cocaine, no FRET signal was observed due to the release of the Cy5-oligonucleotide after analyte binding. The signal-off assay achieved an LOD of 0.5 μM for cocaine, which is comparable to other electrochemical and enzyme-based assays. The generally low sensitivity was explained by the poor affinity of the aptamer towards cocaine. Additionally, a signal-on assay was designed by forming a sandwich of a 3′-biotinylated oligonucleotide and 5′-Cy5-oligonucleotide, the cocaine aptamer, and a 3′-Iowa-black-oligonucleotide, which quenched the emission of the 605QD/Cy5 FRET. In the presence of cocaine, the quencher containing the oligonucleotide was released, and

the FRET emission between the 605QD and Cy5 was detected. A 488-nm argon laser was focused on the capillary (50 μm inner diameter), and photon bursts of 605QD and Cy5 were detected simultaneously by two avalanche photodiodes (APD).

A high-throughput assay was developed in a very narrow channel (1–2 μm width and height) integrated in a chip system (Figure 10).[89] Semiconducting polymer dots (Pdots) were modified with streptavidin and the binding of biotin-Alexa647 was investigated. Au NPs were added to the solution as an internal standard to compensate for instrumental fluctuations. The platform combined confocal fluorescence detection with narrow channels, which made it possible to count photon bursts corresponding to individual NP-labeled molecules. Additionally, the dual laser excitation scheme enabled the quantification of the number of fluorophores per NP. This is a very promising technique for the characterization of different nanoconjugates.

5.1.3. *Fluorescence Correlation Spectroscopy*

To distinguish two components by FCS, at least a twofold difference in their diffusion coefficients is required, which corresponds to approximately an eightfold mass difference (in the case of an idealized compact hydrodynamic sphere).[90] This can be a limiting factor for the analysis of associations of particles with similar mass. If small fluorescent label molecules are replaced by larger NPs, however, the difference in the diffusion times between the free immunoreagents and the formed immunocomplex increases, and the sensitivity of FCS is improved. For example, a sandwich aptamer-based FCS assay utilizing QD-based probes was reported for the detection of thrombin in serum with an LOD of 2.6 nM and a working range of 5–500 nM.[91]

The general configuration of the FCCS requires the alignment of the two lasers with different wavelengths to the same focal spot, which makes the optical setup more complicated than the conventional single-laser FCS. The misalignment of the detection volumes can lead to a decrease of apparent cross-correlation. The single-wavelength excitation FCCS (SW-FCCS) developed by Wohland's group[92] overcame this limitation by the use of two probes, which can be excited using the same wavelength, but their emission is separated due to a large difference of the Stokes shifts. This can be conveniently achieved by the use of QDs[93] or long Stokes shift fluorescent proteins.[94] The group of Ren[95] designed sandwich and competitive assays based on SW-FCCS for the detection of alpha-fetoprotein (AFP). In both approaches, 655QDs (655 nm emission) and Alexa Fluor 488 (520 nm emission) were chosen as the labels. The achieved LODs were 20 pM (sandwich assay) and 180 pM (competitive assay).

5.2. *Photon-Upconversion Nanoparticles*

The optical background of traditional fluorescence readout can be avoided by using photon-upconversion nanoparticles (UCNPs) that emit shorter-wavelength light under near-infrared (NIR) excitation (anti-Stokes emission).[96] UCNPs are lanthanide-doped nanocrystals and the most efficient UCNPs consist of a hexagonal $NaYF_4$ host crystal doped with Yb^{3+} and Er^{3+} or Tm^{3+}. The anti-Stokes emission strongly reduces autofluorescence and light scattering. Fur-

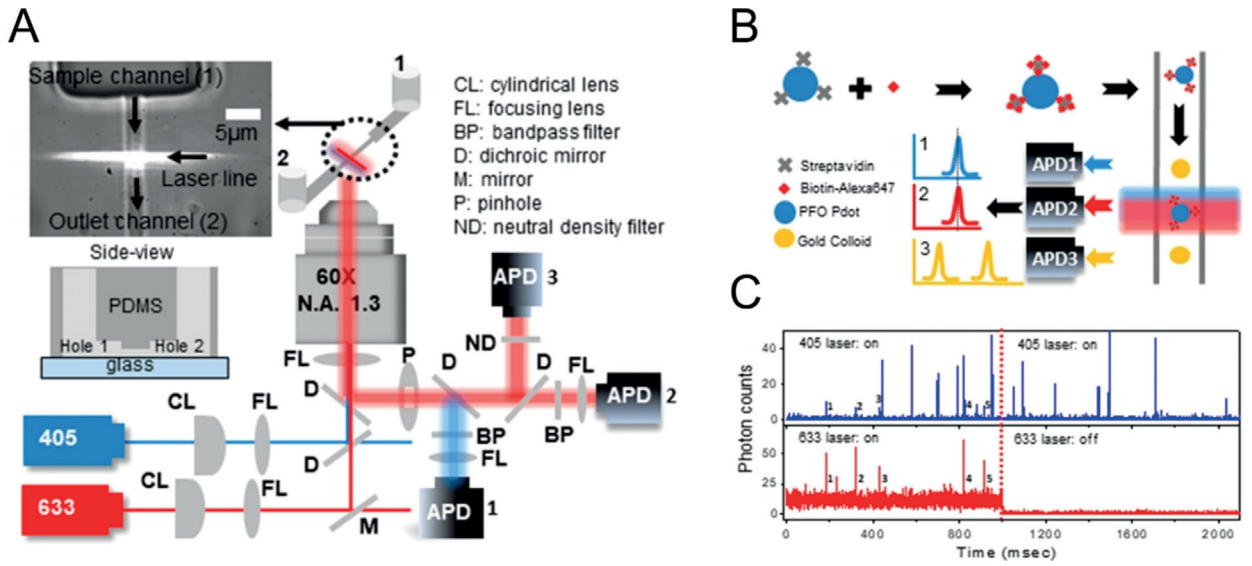

Figure 10. A) Optical setup of the single-particle flow platform. Avalanche photodiodes APD1 and APD2 detect the fluorescence of Pdots and Alexa647, respectively, while APD3 detects the backscattered light of Au NPs. B) Labeling and measurement procedure to quantify the number of streptavidin molecules bound to the surface of Pdots. C) Fluorescence intensity traces of single-particle flow measurements of the Pdot-SA-biotin-Alexa647 complex. Blue (top) and red (bottom) traces are from Pdots and biotin-Alexa647, respectively. The dotted red line indicates the time at which the 633 nm laser was turned off. The five labeled peaks indicate the Pdot-SA-biotin-Alexa647 complex since both blue (Pdot) and red (biotin) fluorescence were detected simultaneously. Reprinted with permission from ref. [89]. Copyright 2018 American Chemical Society.

ther advantages of UCNPs include a high photostability and multiple and narrow emission bands that can be tuned individually for the multiplexed detection of several analytes in parallel.[97] For example, the group of Soukka[98] developed a multiplexed array-in-well assay to determine the immune status against virus infections in human serum samples by the spatial arrangement of several virus antigens on a microtiter plate. Additionally, two types of UCNP labels with different emission colors (Er-doped: green; Tm-doped: blue) were used to distinguish between IgG and IgM antibody classes.

The groups of Fan[99] and Jin[100] further enhanced the multiplexing capabilities of UCNPs by combining wavelength- and lifetime-based encoding. The combination of several lifetime populations and emission bands laid the foundation for a very high encoding capacity. This approach was used for the detection and differentiation between the DNA of nine subtypes of human papillomavirus,[99] but can also be readily adapted for multiplexed antibody-based assays.

5.2.1. Detection of Surface-Immobilized Analytes

We have developed a method for visualizing individual UCNPs ($NaYF_4$:Yb^{3+},Er^{3+}) by conventional epiluminescence microscopy and applied it for the sensitive detection of the cancer marker PSA.[22a] Individual sandwich immunocomplexes consisting of 1) an anti-PSA antibody immobilized on the surface of a microtiter well, 2) PSA, and 3) an anti-PSA antibody–UCNP conjugate were counted under an upconversion wide-field microscope equipped with a 980-nm laser excitation source (Figure 11). The single-molecule (digital) ULISA provided an LOD of 1.2 pg mL^{-1} (42 fM) PSA in 25% blood serum and covered a dynamic range of three orders of magnitude. The digital readout provided single-particle resolution without instrumental background, which resulted in ten times lower LOD compared to the classical (analog) readout of luminescence intensity. An important advantage of the digital readout is the resistance against NP aggregation. In the analog mode, a large aggregate containing hundreds of luminescent NPs can lead to a very high background signal. By contrast, in the digital mode, each aggregate—regardless of its size—only counts as a single binding event and has only a marginal effect on the background signal. Recently, we have prepared a detection label based on a conjugate of PEG-coated UCNPs with streptavidin, which allowed to decrease the label concentration and further improved the LOD by a factor of 50 to ≈20 fg mL^{-1}.[22b]

Li et al.[101] designed a digital homogeneous sandwich immunosorbent assay based on UCNPs ($NaYF_4$:Yb^{3+},Er^{3+}, 42 nm in diameter) for PSA. An antibody-coated UCNP, PSA, and an antibody-coated Au NP formed an immunocomplex. As the green upconversion luminescence overlapped strongly with the absorption spectrum of 50 nm Au NPs, luminescence energy transfer (LRET) strongly quenched the upconversion luminescence. Consequently, the ratio of the visible particles in a flow cell and the amount of UCNPs that was visible in the negative control decreased. The assay achieved an LOD of 1.0 pM in buffer and 2.3 pM in serum.

5.2.2. Fluorescence Correlation Spectroscopy

If a sample such as blood or plasma is strongly autofluorescent, the FCS/FCCS signal of a label present in subnanomolar concentrations is not detectable due to spectral overlap. This effect can either be reduced by using brighter labels or by measuring the cross-correlation of UCNP labels to avoid optical background interference. Lahtinen et al.[102] developed an assay based on upconversion cross-correlation spectroscopy for the detection of thyroid-stimulating hormone (TSH). Green ($NaYF_4$:Yb^{3+},Er^{3+})- and blue ($NaYF_4$:Yb^{3+},Tm^{3+})-emitting UCNPs were conjugated with anti-TSH antibodies, and the cross-correlation was measured upon binding of the analyte TSH. Compared to small organic fluorophores, NP labels have a higher tendency to form aggregates, bind non-specifically, and induce bridging of more

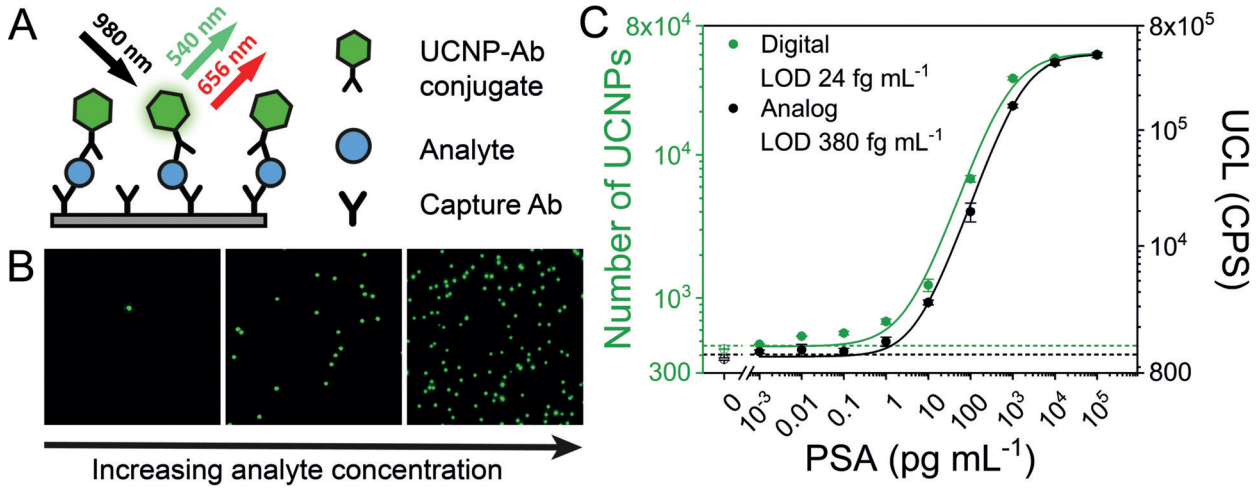

Figure 11. Single-molecule ULISA. A) Scheme of sandwich immunoassay; Ab = antibody. B) Wide-field upconversion microscope images of single immunocomplexes carrying a UCNP label. C) Calibration curves of the digital (green) and analog ULISA (black). The number of UCNPs is given by the diffraction-limited spots in (B) and the upconversion luminescence (UCL) is recorded by a microtiter plate reader.[22]

than two NPs. To suppress these effects, large intensity bursts that were attributed to aggregates were removed before calculating the auto- and cross-correlation functions.[103] However, the smaller bursts were still causing strong variations of the amplitude, which affected the assay sensitivity. The achieved LOD was 15 mIU L^{-1}, which is above the range of normal TSH concentrations in serum (0.3–5.0 mIU L^{-1}).

5.3. Plasmonic Nanoparticles

Plasmonic NPs have been used in single-molecule immunoassays because they enable a highly sensitive readout based on their light-scattering properties and spectral changes upon analyte binding. The most common materials include gold (Au NPs) and silver (Ag NPs). Au NPs are labels that are most frequently used in immunoassays in general, finding applications in lateral flow assays, electrochemistry, colorimetric assays, and plasmonic sensing.[104] Ag NPs are less stable because they are oxidized more easily, but they possess higher extinction coefficients and stronger Raman and fluorescence enhancement.[105] In both cases, the plasmonic properties are strongly dependent on the shape and the size of the NP.[106]

5.3.1. Dark-Field Microscopy

Dark-field microscopy is the most common method for the detection of single plasmonic particles. In dark-field microscopy, the illumination light is prevented from entering the objective acceptance cone, whereas the light scattering from immobilized NPs is collected by the objective lens. Background scattering and reflection from interfaces can be further reduced by optimizing the refractive indices.

Poon et al.[107] developed an antibody-based single-particle scattering intensity assay for the detection of various clinical cancer markers such as AFP, CEA, and PSA. A gold nanoprobe coated with a capture antibody was immobilized in a flow cell on microscope coverslips. Then the analyte was added, followed by a second Ag NP carrying the detection antibody. Binding of Au and Ag NPs resulted in a threefold increase of the scattering intensity and a spectral shift. The LODs for all three analytes were in the range of 1 to 6 pM.

Wu et al.[108] developed a magnetic-bead-based sandwich immunoassay for AFP, CEA, and PSA using Au NP detection. First, a sandwich immunocomplex was formed by incubating the sample with a biotinylated antibody and a second unlabeled antibody (Figure 12). The immunocomplexes were captured on streptavidin-coated magnetic beads. Au NPs coated with a secondary antibody were added, and unbound labels were removed by magnetic separation. After washing, the Au NPs were released from the beads by treatment with 8 M urea. The free Au NPs were then immobilized on a cationic coverslip and counted under a dark-field microscope. Zhu et al.[109] developed a similar sandwich immunoassay for PSA using a preconcentration step on magnetic beads.

The Gooding group[110] showed the potential use of commercial cameras as they appear in smartphones for the high-throughput spectral readout of the localized surface plasmon resonance (LSPR) spectra of up to 5000 individual Au NPs (Figure 13). Anti-interleukin-6 (IL-6) antibodies were conjugated to Au NPs and spin-coated on a glass slide. A biotinylated anti-IL-6 antibody was attached to a 10-nm streptavidin-modified satellite Au NP and then added to the Au NPs immobilized on glass. The binding of the satellite Au NP resulted in a redshift of the LSPR signal due to plasmon coupling. The spectral shift of single Au NPs before and after the addition of IL-6 was used to calculate the analyte concentration. While the setup was not sensitive enough to detect single binding events, single-molecule sensitivity may be achieved by using bigger satellite particles (20–80 nm).

A method for extracting affinity constants based on statistical fluctuations in equilibrium was proposed by Luthgens and Janshoff.[111] It is based on a single-molecule readout of an array of isolated sensors, which can accommodate a high amount of simultaneously bound analyte molecules. Aćimović et al.[112] employed this principle to follow antibody–antigen binding kinetics on long timescales on the single-molecule level. First, Au nanorods were modified with

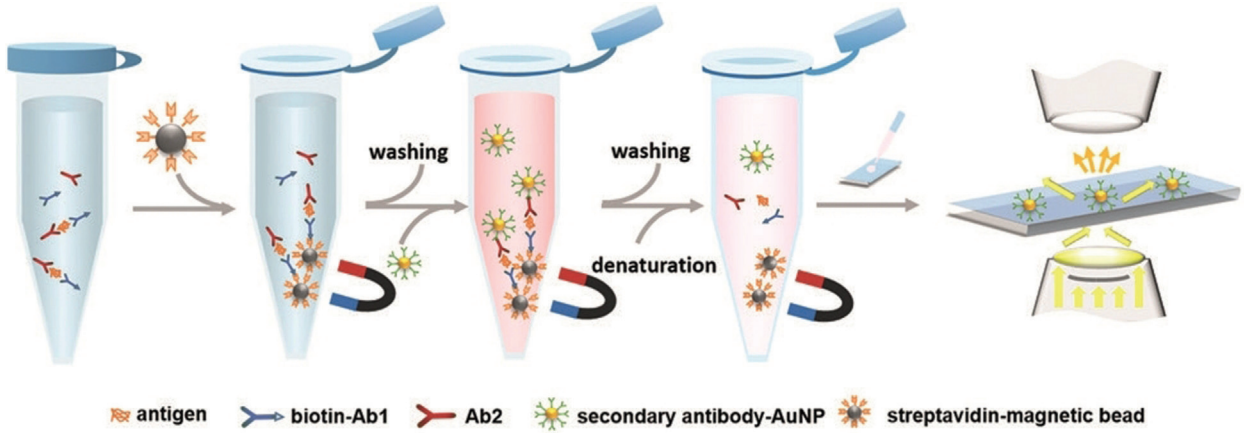

Figure 12. Au NP-based detection of PSA with dark-field microscopy readout. Reprinted with permissions from ref. [108]. Copyright 2017 Royal Society of Chemistry.

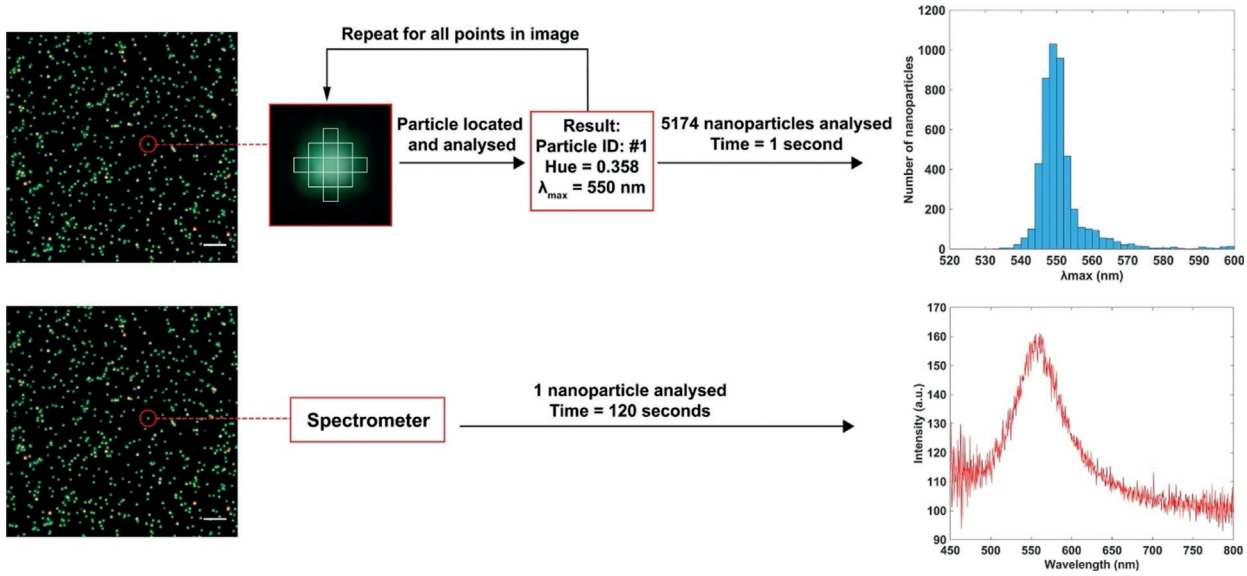

Figure 13. Top: Color analysis using a commercial camera. The color of the Au NPs is transformed into a hue value that corresponds to a specific wavelength and plotted in a histogram. Bottom: Color analyses using a spectrometer; each spot has to be processed individually. Reprinted with permission from ref. [110]. Copyright 2018 Elsevier.

thiolated PEG followed by binding of an anti-PEG antibody. The signal fluctuations at equilibrium enabled the calculation of kinetic parameters and analyte concentrations.

Yang et al.[113] developed a digital aptamer-based assay for the detection of thrombin. A biotinylated anti-thrombin aptamer was immobilized on streptavidin-coated magnetic beads. Au NPs coated with a DNA sequence complementary to the aptamer were introduced and bound to the aptamer. In the presence of thrombin, the Au NPs were released, and the beads were magnetically separated. The free Au NPs in the supernatant were either counted individually under a dark-field microscope by dispersing a drop on a coverslip (digital detection) or—at high concentrations—by measuring the absorption resulting from NP aggregation (analog detection). Another aptamer-based thrombin assay was developed by Li et al.[114] A glass slide was modified by Au NPs to bind a thrombin-specific aptamer. Thrombin was specifically captured, followed by another anti-thrombin aptamer to form a sandwich complex. After the addition of Au NPs, NP oligomers formed through Au–S binding, and the color changed from green to yellow and red. Individual NPs were detected under a dark-field microscope, and the thrombin concentration was estimated from the intensity change of the Au NPs. The assay detected thrombin with an LOD of 10 fM.

Chen et al.[115] increased the LSPR signal of individual Au NPs by enzymatic amplification. When a single streptavidin horseradish peroxidase conjugate bound to a biotinylated Au NP, the resulting LSPR shift enabled the detection of single molecules. The enzymatic precipitation of 3,3′-diaminobenzidine further increased the colorimetric response by a factor of 50. This method can potentially be developed into a sandwich immunoassay by coating the Au NPs with a capture antibody and conjugating horseradish peroxidase with a detection antibody.

5.3.2. *Light Scattering Correlation Spectroscopy*

Resonance light scattering correlation spectroscopy (RLSCS) measures the fluctuations of resonance light scattering in small volumes due to the Brownian motion of single NPs. Noble metal NPs are excellent labels for RSLCS because of their efficient resonance light scattering, which is several orders of magnitude higher than scattering of small organic molecules.[116] The RSLCS instrumentation is similar to that of FCS, but no emission filter is needed. Like FCS, the RLSCS immunoassays are based on the increase of the characteristic diffusion time in the detection volume due to the formation of an immunocomplex. RLSCS was used in a sandwich immunoassay for AFP (LOD 1 pM)[117] and in competitive assays for AFP (LOD 100 pM) and 17-β-estradiol (LOD 10 pM).[118] Similar to FCS and FCCS, one of the major limitations of RLSCS is the significant effect of NP label aggregation. Although in both studies the particles were coated by PEG to suppress the NP aggregation, in the presence of a real sample matrix, the assay reproducibility in serum was lower compared to the standard ELISA.

Fluorescence and scattering light cross-correlation spectroscopy (FSCCS) was used by Wang et al.[119] in a confocal setup for measuring the scattering of labels based on Au NPs and a fluorescent dye (Alexa Fluor 488) as a probe pair (Figure 14). The advantage of FSCCS is the use of a single 488-nm laser as the excitation source for both the Au NP and the fluorescent label. A sandwich immunoassay based on this setup achieved an LOD of 3.1 pM AFP.

5.3.3. *Surface Plasmon Microscopy*

The adsorption of individual plasmonic NPs can be followed in real time using surface plasmon microscopy.[120] Changes in surface plasmon resonance (SPR) properties

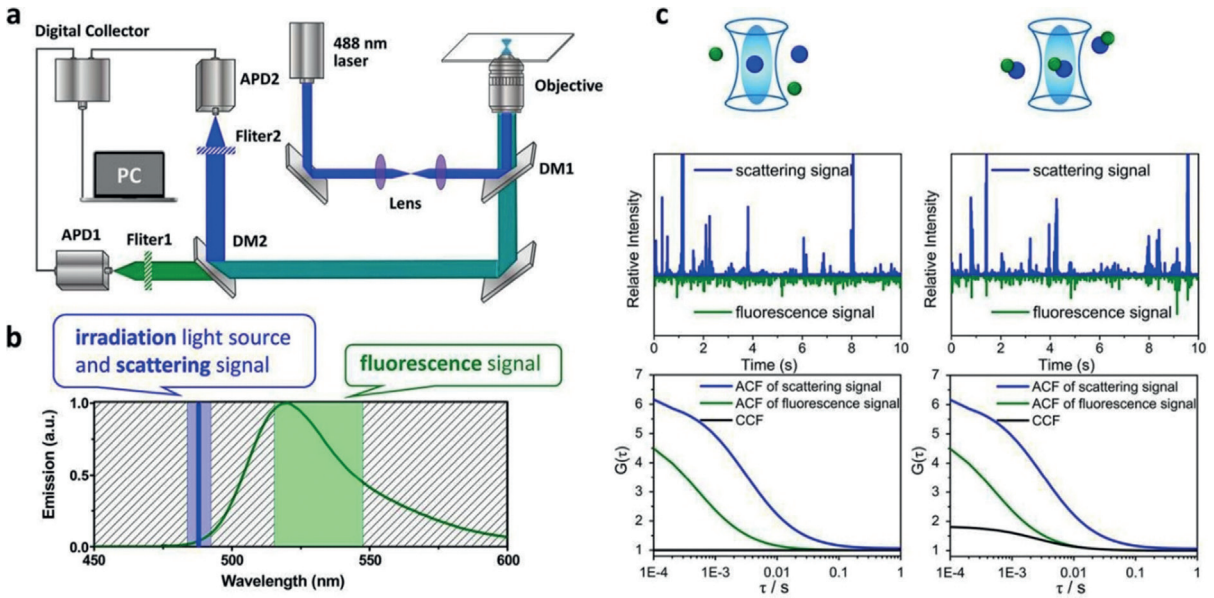

Figure 14. a) Setup for FSCCS. b) Spectral separation of excitation and emission wavelengths. c) Scattering and fluorescence signals and their correlation curves for labeled species diffusing independently (left) or linked (right). ACF = autocorrelation curve, CCF = cross-correlation curve. Reprinted with permission from ref. [119]. Copyright 2017 American Chemical Society.

affect the reflected light intensity, which is detected by an image sensor.[121] The measurement can be based either on the setup with a high-NA microscope objective[122] or on the standard Kretschmann configuration.[123] While a high-NA objective provides high resolution, the field of view is typically limited to an area of 0.01 mm^2. On the other hand, the Kretschmann configuration provides a wider field of view (over 1 mm^2), but imperfections in the arrangement of object, lens, and image planes degrade the performance and resolution of the optical system. SPR imaging is typically used for the characterization of homogenous films, where high resolution is not necessary.[124]

The group of Mirsky developed a wide-field approach for the detection and quantification of single NPs[121] and applied it for the analysis of Au and Ag NPs in complex samples such as wine, apple juice, and sunscreen (Figure 15).[125] The large imaging area of the wide-field setup increased the probability of detecting single NP adsorption events at low concentrations. The signal strength was mainly determined by the size and refractive index of the NPs, the distance from the plasmonic substrate, and the performance of the optical system. The adsorption of a single NP, however, only led to a small signal change. To enhance the sensitivity, differential images of local temporal and spatial intensity changes were evaluated based on the changes between the two subsequently captured frames. The method provided an LOD of 10^6 NPs mL^{-1} ($\approx$1.6 fM) and a working range of 10^6–10^{10} NPs mL^{-1} with a measurement time of 1 min. The sensitivity can be further improved by increasing the analysis time or the sensing surface area.

Furthermore, the combination of surface plasmon microscopy with electrochemical analysis made it possible to determine the composition of NPs.[126] This technique was applied to the analysis of Ag and Cu NPs and achieved an LOD of 10^4 NPs mL^{-1}. Surface plasmon microscopy was also employed for single-molecule detection of DNA hybridization,[127] and the application to single-molecule immunoassays would be straightforward.

5.3.4. *Detection in Microarrays*

Sevenler et al.[128] used Au nanorods as labels for the detection of hepatitis B virus surface antigen (HBsAg) on a protein microarray. An anti-HBsAg antibody was spotted on an interferometric reflectance imaging sensing (IRIS) substrate and incubated with the antigen, followed by the addition of Au nanorods coated with another anti-HBsAg antibody, and the particles were counted in an automated imaging device under illumination by circularly polarized light. Light reflected by the IRIS substrate was also polarized, but the light scattered by Au nanorods was linearly polarized along the longitudinal axis of the NPs and was separated from the reflected light. The assay achieved an LOD of 3.2 pg mL^{-1}.

Belushkin et al.[129] designed a sandwich immunoassay for C-reactive protein (CRP). A gold nanohole array was coated with an anti-CRP capture antibody. The array was immersed in the analyte medium, washed, and immersed in a dispersion of Au NPs that were coated with an anti-CRP antibody. Au NPs in or close to the nanoholes could be detected because of a decrease in the extraordinary optical transmission (EOT). EOT is an SPR-based phenomenon that occurs when light passes through a subwavelength-sized regularly shaped metallic film. Particles too far away from nanoholes were not detected. Single Au NPs were counted under a microscope.

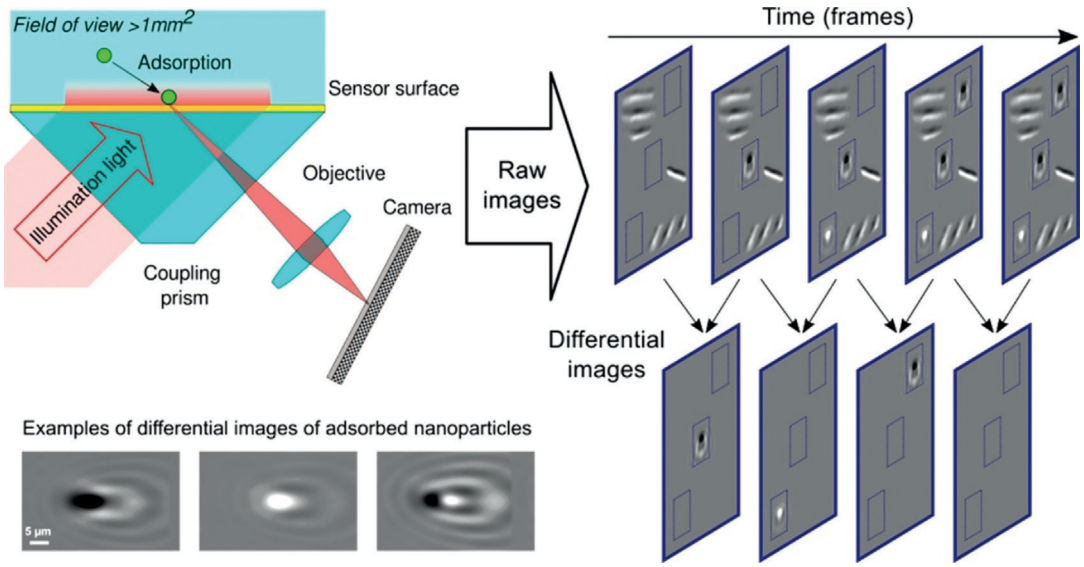

Figure 15. Surface plasmon microscopy for the detection of single NPs adsorbing to the sensor surface. Reprinted with permission from ref. [125]. Copyright 2016 American Chemical Society.

6. Bead Labels

6.1. Fluorescence Microscopy

While it is not possible to make a sharp separation between NPs and beads, here we define beads as labels larger than 100 nm in diameter. The larger size, on the one hand, offers an easier way for detection but, on the other hand, impedes the accessibility of the label to the analyte. The Lövgren group[130] was one of the first to employ a bead label for the detection of single analyte molecules. Individual europium-doped beads—with a diameter of 107 nm, very close to NP size—were detected by time-resolved fluorescence (TRF). A microtiter plate was coated with a monoclonal anti-PSA antibody and biotinylated PSA was added, followed by the streptavidin-coated Eu beads. The analyte binding was measured in the analog mode by time-resolved fluorometry and in the digital mode by counting single bead labels under a time-resolved microscope equipped with a 10× objective and a CCD camera. The assay achieved an LOD of 0.38 pg mL^{-1} of biotinylated PSA.

Wu et al.[131] used color-encoded magnetic beads to simultaneously detect single virus particles of three different types of avian influenza (Figure 16). Polystyrene beads were coated first with γ-Fe_2O_3, then with QDs displaying different emission colors (green, yellow, red) and with antibodies against avian influenza. The three bead types, each one specific for a certain avian influenza type, were dispersed in the sample and magnetically separated. The beads were then loaded onto a PDMS microarray that was coated with antibodies for the different virus types. After washing, only beads that captured a virus particle remained in the array. The assay resulted in an LOD of 0.02 pg mL^{-1}.

Zhang et al.[132] embedded UCNPs of different colors and in different ratios into polymer microbeads to generate codes for the multiplexed detection of DNA. The combination of n intensity levels with m colors resulted in (n^m−1) unique codes. The labels were detected at the single-bead level under 980-nm excitation by confocal microscopy. The DNA sequence was identified based on the upconversion encoding signal, while the presence and amount of the target sequence was indicated by conventional fluorescent dyes.

Gite et al.[133] developed a sandwich assay consisting of 1) a magnetic particle, 2) an anti-*Clostridium difficile* capture antibody, 3) *C. difficile,* 4) an anti-*C. difficile* detection antibody, and 5) a fluorescent microparticle. A mixture of a visible-light-absorbing dye-cushion reagent and the density agent iodixanol was dried on the bottom of each microwell (Figure 17). The immunoreagents were added, and the magnetic beads were pulled to the bottom of the microplate with a magnet. The dye absorbed all visible light and stayed at the bottom due to the density agent, resulting in a strong reduction of the background fluorescence of unbound fluorescent particles. Single fluorescent beads appeared as bright pixels on a digital camera chip.

6.2. Bright-Field Microscopy

Tekin et al.[134] developed a microfluidic-based magnetic bead counting assay for the detection of proteins in serum (Figure 18). Magnetic beads (2.8 µm) were modified with a capture antibody to preconcentrate a target protein from fetal bovine serum. The beads were passed over over a glass surface patterned with smaller antibody-modified magnetic beads (1 µm). The larger beads were attracted to the surface by a magnetic field, which allowed them to "roll" over multiple smaller beads due to dipolar magnetic forces. An immunocomplex formed when the antigen had a suitable orientation on the bead. The drag force caused by the flow had to be strong enough to release the particles when only dipolar forces were present. The analyte concentration was

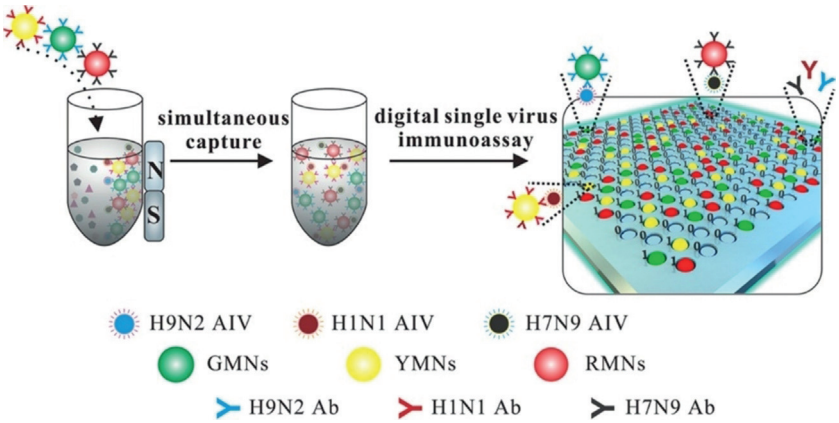

Figure 16. Scheme of the multiplex assay for avian influenza viruses. Color-encoded magnetic spheres—each coated with a specific anti-avian influenza virus antibody—are dispersed in the virus sample. After magnetic purification, the particles are loaded onto a PDMS array and digitally counted. Reprinted with permission from ref. [131]. Copyright 2019 American Chemical Society.

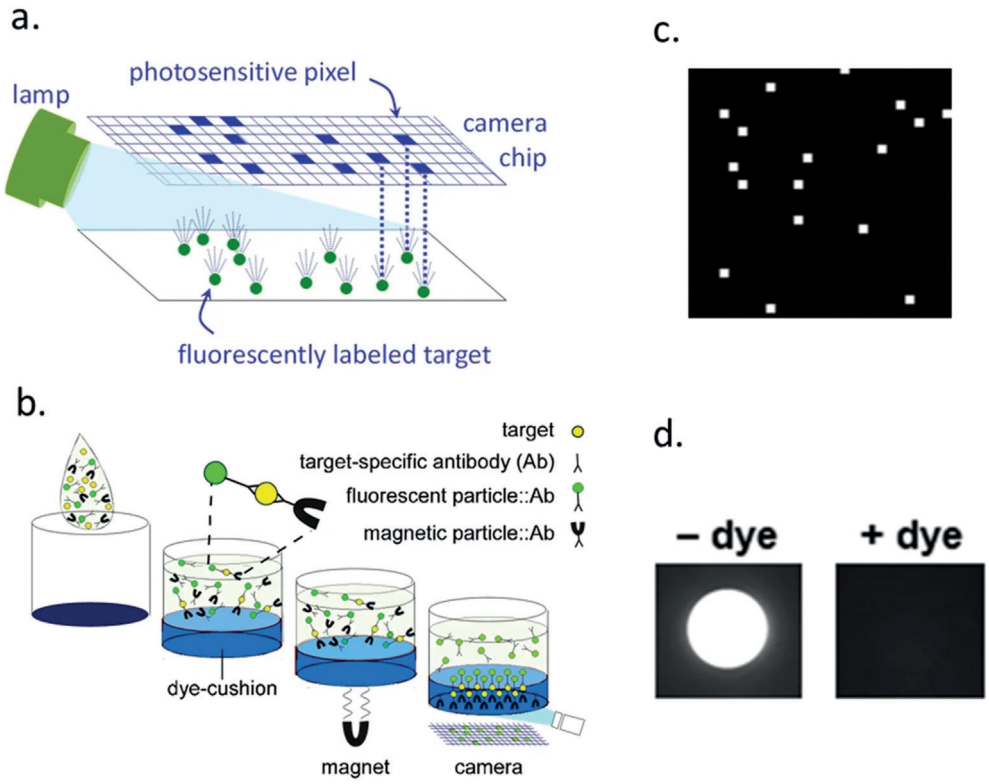

Figure 17. a) Detection of single fluorescent beads on one or a small group of pixels of a camera chip without the need for microscope magnification. b) After immunocomplex formation, a magnet immobilizes the magnetic beads at the bottom of a microwell. Only fluorescent beads near the surface are excited because the dye absorbs the excitation light that penetrates deeper into the well. c) Fluorescent beads appear as bright pixels on the digital camera. d) A comparison of a well with and without dye shows the efficiency of a dye-cushion layer. Reprinted from ref. [133] with the permission of Creative Commons Attribution 4.0 International License.

determined by counting the bound large beads on a conventional optical microscope. The combination of a magnetic preconcentration step and digital counting of bound magnetic beads in a microfluidic chip afforded an LOD of 60 aM ($\approx$1 fg mL^{-1}) TNF-α, equivalent to $\approx$200 molecules in 5 μL of the sample.

6.3. Dark-Field Microscopy

Tethered particle monitoring is a biophysical technique used to characterize changes in the length of a polymer tethered to a particle on one end and a surface on the other end. The Brownian motion of the particle limited by the tether is usually monitored optically. Schafer et al.[135] introduced tethered particle monitoring in 1991 to follow the transcription of a DNA template bound to an Au NP by RNA polymerase immobilized on a glass slide. Various modifications of the principle are possible and can be used for monitoring single-molecule binding events in an immunoassay.

Visser et al.[136] utilized the tethered particle monitoring in an aptamer-based sandwich assay for thrombin. Magnetic beads were modified with an anti-thrombin capture aptamer and the glass surface of a flow chip was modified by a detection aptamer. The beads were tethered to the glass surface by a 40-nm-long dsDNA strand. When the analyte was captured between the aptamers, the bead was anchored onto the surface, and its mobility was strongly reduced (Figure 19), which was monitored over time by dark-field microscopy. The binding and unbinding events of hundreds of beads were detected simultaneously. The rate of switching between the two states, and especially the lifetime of the unbound state, was dependent on the concentration of thrombin in a range of 10–300 nM. As the interaction was reversible and all recognition elements were bound in the flow cell, the system is amenable for continuous biomarker monitoring.

Silver et al.[137] developed a sandwich immunoassay for the detection of PSA based on tethered particle monitoring. Magnetic beads (2.8 μm) with immobilized antibody captured

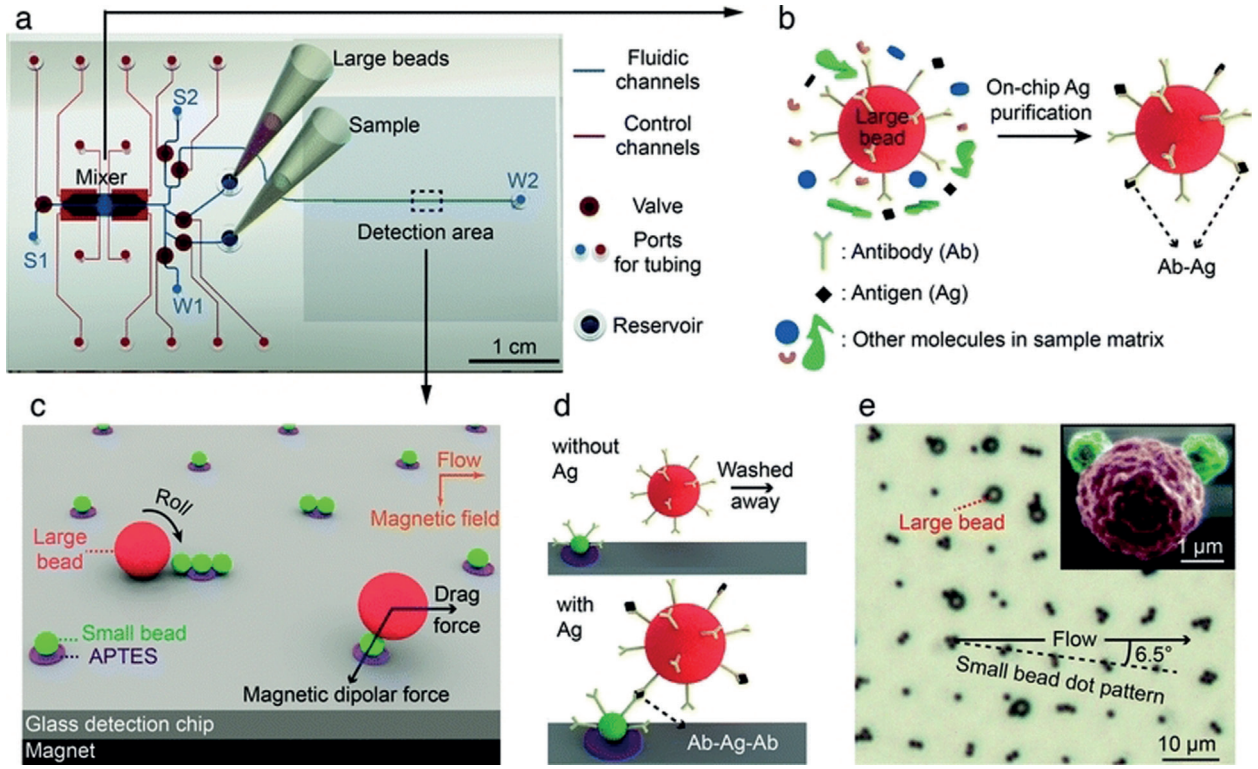

Figure 18. Microfluidic-based magnetic counting assay. a) Scheme of a microfluidic chip. b) Large magnetic beads separate the target protein from the matrix. c) The large beads roll over the patterned array of smaller beads that are magnetically attracted to the surface. d) A sandwich immunocomplex is formed when the antigen and the large bead have a suitable orientation. e) Optical micrograph of the captured large beads on the patterned array of small beads. A colored SEM photograph in the inset shows the large bead captured on the small beads. Reprinted with permission from ref. [134]. Copyright 2013 Royal Society of Chemistry.

PSA from the sample matrix. After magnetic separation, the beads were incubated with the biotinylated detection antibody and introduced into a flow cell. The beads carrying the immunocomplex were captured by a streptavidin-terminated DNA tether. This tether allowed the beads to move 12 μm back and forth when the flow direction was changed by manual syringe operation. Thus, specifically bound beads were distinguished from nonspecifically bound beads and counted using a low-magnification (10×) dark-field microscope. The assay achieved an LOD of 1 pM PSA.

Akama et al.[138] combined tethered particle monitoring with an immunoassay in femtoliter arrays. In the "digital homogeneous non-enzymatic immunosorbent assay" (HoNon-ELISA), antibody-decorated magnetic particles were used to separate the analyte from the sample matrix. Then, they were magnetically pulled into the microreactors of a femtoliter array chip for the confinement of the antibody–antigen reaction. The antigen was recognized by another antibody immobilized through a PEG linker to the well surface. The sandwich complex tethered the particle to the surface and limited its Brownian motion, which was monitored for thousands of wells in parallel using bright-field or dark-field microscopy and particle tracking analysis. According to the movement patterns, selectively captured particles were discerned from nonspecifically bound ones, and individual binding events were counted. The procedure did not require any washing or signal amplification steps and reached an LOD of 0.093 pg mL^{-1} PSA.

7. Label-Free Detection

Most label-free detection schemes are based on plasmonic effects. While Section 5.3 describes the use of plasmonic NPs as labels, here we focus on the arrangement of plasmonic nanostructures to generate local hot spots, which are very sensitive to analyte binding.[139] Localized surface plasmon resonance (LSPR) has been used to follow the changes of local refractive indices near plasmonic NPs. There are various possibilities to link the refractive index changes to the presence of the analyte, as demonstrated by numerous reports of bulk LSPR-based immunoassays.[20a,140] The high sensitivity of LSPR can be exploited to characterize statistical distributions of molecular properties and to follow single-molecule binding events.[141] Beuwer et al.[142] used correlated atomic force microscopy (AFM) and optical microscopy to study how the binding location affects the changes of LSPR signals. Au NPs were used as a model analyte and bound to single-crystal Au nanorods using cysteine–cysteine coupling.[143] In the correlative approach, AFM was used to study the binding locations, and the plasmon shifts were evaluated by single-particle spectroscopy. A broad distribution of LSPR shifts was

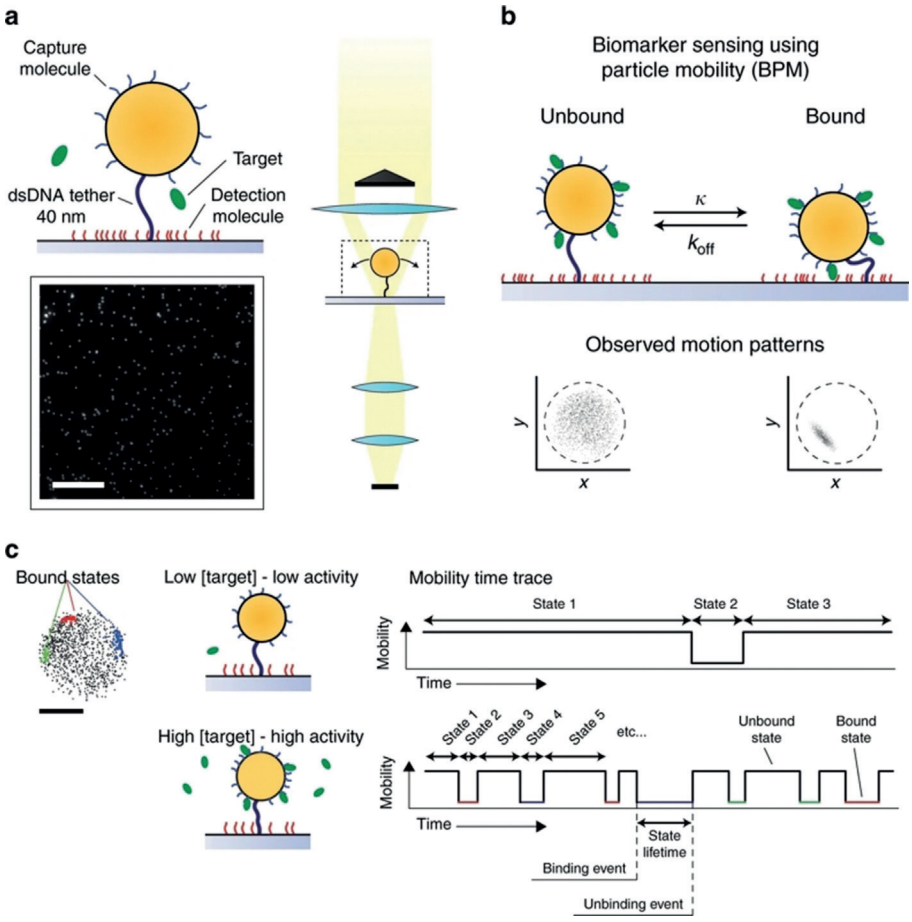

Figure 19. Tethered particle monitoring. a) Particles (orange) are modified by capture aptamers (blue) and tethered to the substrate by a 40-nm dsDNA strand (black). The substrate is decorated with detection aptamers (red). The image was recorded by dark-field microscopy (scale bar: 50 μm). b) After thrombin (green) binding, the particle's movement is restricted, which changes the motion pattern. c) The particle mobility is continuously analyzed for hundreds of particles in parallel. The mobility time traces of low and high analyte concentration reveal individual binding and unbinding events. Reprinted from ref. [136] with the permission of Creative Commons Attribution 4.0 International License.

observed for similar binding locations, which was attributed to the size dispersion of the Au NPs. Binding of the Au NPs to the tip of the rod led to stronger plasmon shifts than binding to its sides. Since the probability of binding to various locations of a nanorod differs,[144] the knowledge of the binding location can help not only to determine the level of sensor response but also to evaluate the binding constants. Site-specific functionalization techniques can be used to maximize the sensitivity and reduce the signal distribution.[145] Lee et al.[146] designed plasmon rulers as sensors for the detection of single molecules of matrix metalloproteinase (MMP3). When two noble metal NPs exhibiting LSPR approach each other, their individual surface plasmon resonances couple, which generates a shift in the scattering spectrum and can be detected by dark-field microscopy.

Beuwer et al.[147] used Au nanorods to detect the interaction of biotin and an anti-biotin antibody (Figure 20). They functionalized the tips of Au nanorods with thiolated biotin and detected the change in the scattering intensity of individual nanorods. When the plasmon wavelength of a particle was shorter than the 795-nm illumination light, the scattered signal increased upon antibody binding. The intensity change was stepwise and irreversible due to the strong biotin–antibody interaction. The binding constants were calculated from the mean waiting times and followed a Poisson distribution. The LOD was influenced by the number of binding events in a certain timeframe. As low analyte concentration resulted in long waiting times, a high number of particles had to be observed, which was limited by the field of view of the objective (ca. 50000 NPs). The high rate of binding events at high analyte concentrations required a fast camera image acquisition. The shorter exposure times were compensated by a higher excitation power, which was limited by photothermal heating of the particles.

Another emerging label-free technique for the detection of single molecules are whispering gallery mode (WGM) microring resonators, which trap light due to multiple total internal reflections at a curved boundary (Figure 21). Analyte binding to the optical ring resonators results in a shift of the resonance wavelength. Arrays of microring resonators were used for the multiplexed detection of five protein biomarkers.[148] Single-molecule sensitivity for protein or DNA has been achieved. More recently, even single ions such as Hg^{2+} and Zn^{2+} have been detected using a gold antenna coupled to a WGM microresonator.[149]

Surface-enhanced (SERS) and tip-enhanced Raman spectroscopy (TERS) also enable the label-free detection of single protein molecules.[151] It is, however, difficult to employ these techniques for measuring protein concentrations in routine analytical applications.

8. Summary and Outlook

As new and low-abundance disease markers are investigated, there is a growing need for developing more sensitive detection methods. Tables 1–3 summarize various assay types for the digital readout of analytes that have been discussed in the Review.

Single-molecule immunoassays have gained popularity in clinical research and diagnostics and some platforms have

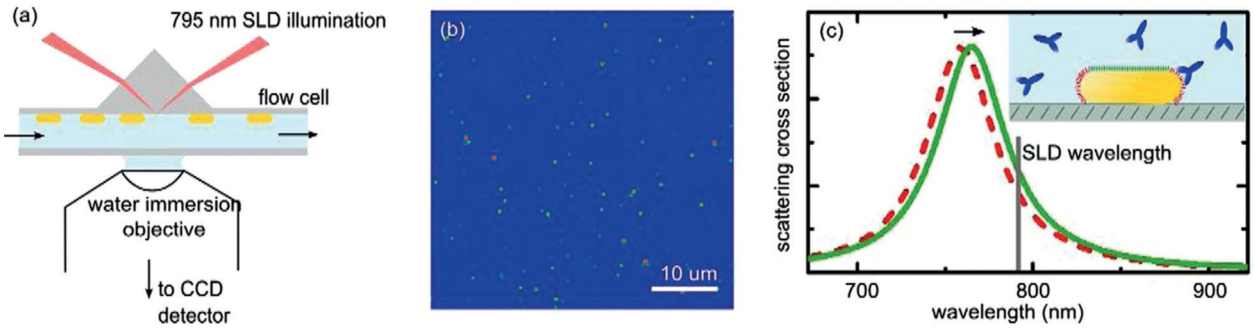

Figure 20. a) Scheme of a dark-field microscope with a superluminescent diode (SLD). b) Image of surface-immobilized gold nanorods shown in pseudocolors. c) The tips of the gold nanorods are functionalized by receptors (red), while the sides are blocked by tetraethylene glycol (green). An individual antibody-binding event results in a redshift of the plasmon resonance. The vertical gray line indicates the SLD center wavelength. Reprinted with permission from ref. [147]. Copyright 2015 American Chemical Society.

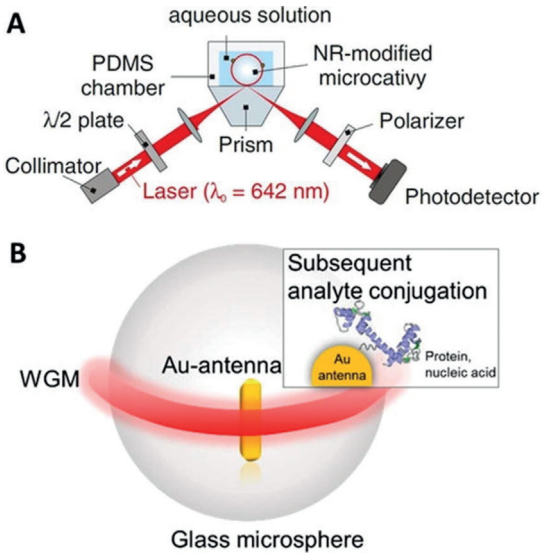

Figure 21. Scheme of optical ring resonators. A) Instrument setup for coupling a laser into an optical ring resonator. B) A glass microsphere serves as an optical microcavity to measure physical, chemical, and biological properties. Near total internal reflection of light results in an optical resonance (WGM, red). The WGM couples to a gold nanorod where it excites plasmon resonance. Single analyte molecules can be detected if they bind inside plasmonic hot spots. Reprinted with permission from ref. [150]. Copyright 2017 IOP Publishing.

been commercialized. Commercial single-molecule immunoassays offer complete solutions for the detection of a wide range of biomarkers in clinical research, including cytokines, hormones, and signaling proteins. As of September 2019, Merck offered 49 ready-to-use immunoassay kits for the Erenna system,[152] and Quanterix offered 130 kits for the Simoa platform.[153] Furthermore, custom development services and kits for in-house development of new assays by the customer are available.

Although the detection of individual optical labels is relatively easy using state-of-the-art detectors, it is still a challenge to achieve the superior sensitivity of single-molecule assays compared to that of analog assays. Recently, the advantages of analog and digital detection modes have been compared systematically using the same TIRF platform.[154] Furthermore, the same analyte was used to evaluate the performance of different assays.[155] Three immunoassay platforms were assessed regarding their ability to detect subpicomolar concentrations of the protein biomarker GAD65.[156]

Another important challenge is the simplicity and robustness of the assay procedure. Even though single-molecule assays can reach extremely high sensitivity, the need for highly sophisticated instrumentation, well-trained personnel, and long operation times can impede their commercialization. Despite these challenges, single-molecule assays are finding their way into real-world applications and can replace conventional methods such as the ELISA or electrochemiluminescence assays. The possibility to detect only a few biomarker molecules in a sample opens up many new possibilities for enhanced diagnostics.

Acknowledgements

We thank Julian Brandmeier for his help with the German translation. H.H.G. acknowledges funding from the German Research Foundation (DFG Heisenberg Program: GO 1968/7-1). This work was further supported by the Ministry of Education, Youth and Sports of the Czech Republic within the program INTER-ACTION (LTAB19011).

Conflict of interest

The authors declare no conflict of interest.

[1] a) S. Weiss, *Science* **1999**, *283*, 1676–1683; b) W. E. Moerner, D. P. Fromm, *Rev. Sci. Instrum.* **2003**, *74*, 3597–3619; c) C. Joo,

Table 1: Digital assays for cancer biomarkers. The LODs were converted into molar concentrations wherever applicable.

Assay type	Analyte	Matrix	LOD	Working range	Assay time (min)	Sample volume	Ref.
FCCS with QDs	AFP	buffer	20 pM	20 pM–5 nM	120	10 μL	[95]
Resonance light scattering correlation spectroscopy	AFP	buffer	1 pM	1 pM–1 nM	50	20 μL	[117]
Fluorescence and scattering light cross-correlation spectroscopy	AFP	buffer	3.1 pM	5–580 pM	120	10 μL	[119]
Light scattering correlation spectroscopy	AFP	buffer	100 pM	100 pM–10 nM	120	20 μL	[118]
Counting of spatially overlapping two-color QDs	CEA	plasma in buffer	6.1 pM	10.4–666.7 pM	30	n/a	[85]
Droplet microfluidics	exosomes	n/a	17 aM	10 aM–1 pM	n/a	n/a	[52]
Simoa	PSA	25% newborn calf serum in buffer	98 fM	100 fM–500 pM	n/a	n/a	[39]
Droplet array	PSA	buffer	2 aM	1 aM–100 fM	120	n/a	[45]
Femtoliter microfluidic droplets	PSA	buffer	46 fM	0.046–4.62 pM	270	200 μL	[51]
Droplet-based immunoPCR	PSA	buffer	17 pM	17 pM–1 nM	120	30 μL	[58]
Digital ULISA with UCNPs	PSA	25% bovine serum in buffer	42 fM	350 fM–35 pM	150	100 μL	[22a]
Digital ULISA with streptavidin-coated UCNPs	PSA	25% bovine serum in buffer	800 aM	3.5 fM–3.5 pM	210	100 μL	[22b]
Single-UCNP enumeration	PSA	buffer	1 pM	0–500 pM	120	n/a	[101]
Au NP enumeration with dark-field microscopy	PSA	buffer	35 pM	35–700 pM	170	95 μL	[108]
Counting of gold nanorods by dark-field microscopy	PSA	buffer	280 aM	350 aM–350 fM	195	100 μL	[109]
Digital HoNon-ELISA	PSA	buffer	3.2 fM	3.2 fM–3.2 pM	n/a	n/a	[138]
Tethered-bead immunoassay	PSA	buffer	1 pM	1–10 pM	n/a	50 μL	[137]
Simoa	PSA, TNF-α	25% bovine serum	50 aM, 150 aM	100 aM–1 pM	360	100 μL	[38]
Fluorescence-aided multiplexed molecule sorting	CEA, PSA, AFP	50% human serum in buffer	14 pM, 100 pM, 100 pM	10 pM–1 nM, 100 pM–10 nM, 100 pM–10 nM	120	n/a	[73]
Immunoassay based on spectral blueshifts of QDs	CEA, AFP	25% plasma in buffer	6.7 fM, 3.4 fM	10 fM–100 pM	n/a	n/a	[86]
Scattering-based quantitative single-particle intensity measurement	CEA, PSA, AFP	human serum	1.7 pM, 3.3 pM, 5.9 pM	0–300 pM	n/a	n/a	[107]

n/a = not available; AFP = alpha-fetoprotein; CEA = carcinoembryonic antigen; PSA = prostate specific antigen; TNF-a = tumor necrosis factor alpha.

Table 2: Summary of digital assays for other clinical biomarkers. The LODs were converted into molar concentrations wherever applicable.

Assay type	Analyte	Matrix	LOD	Working range	Assay time (min)	Sample volume	Ref.
Fluorescence colocalization	ATP	buffer	100 fM	1 pM–5 nM	45	25 μL	[65]
FCS	contactin-2	17% CSF in buffer	1.5 pM	n/a	60	10 μL	[76]
Microarray-based plasmonic biosensor	CRP	buffer	225 fM	n/a	120	100 μL	[129]
Erenna	cTnI	25% human plasma in buffer	74 fM	n/a	n/a	10 μL	[68]
Bead-based Erenna	cTnI	25% human plasma in buffer	8.7 fM	10 fM–500 pM	180	100 μL	[69]
Light scatting correlation spectroscopy	17-β-estradiol, AFP	buffer	10 pM, 100 pM	10 pM–1 nM, 100 pM–10 nM	120	20 μL	[118]
Single-molecule fluorescence counting	FSH	n/a	34 fM	100 fM–1 nM	n/a	100 μL	[72]
FCCS	hCG PrP	buffer	100 pM 2 nM	100 pM–10 nM (hCG)	40	n/a	[80]
Proximity ligation assay	IL-6	n/a	5 fM	10 fM–1 nM	n/a	n/a	[59]
Counting of Au NPs using dark-field microscopy with digital color analysis	IL-6	buffer	4.76 nM	n/a	n/a	n/a	[110]
Erenna	mutant huntingtin	30% cerebrospinal fluid in buffer	40 fM	40 fM–1 nM	n/a	45 μL	[71]
Simoa	NF-L	25% human serum in buffer	4.3 fM	4.2 fM–26 pM	n/a	152 μL	[42]
Simoa	tau	25% human plasma in buffer	180–250 aM	250 aM–15 pM	n/a	152 μL	[43]
Single-molecule counting fluorescence immunoassay	synthetic Aβ dimers	buffer	0.18 pM	n/a	overnight + 90 min	20 μL	[70]
Aptamer-based assay using QDs	thrombin	buffer	2.6 nM	5–500 nM	60	10 μL	[91]
Core–shell based aptasensor using dark-field microscopy	thrombin	buffer	2.54 fM	6–100 fM	30	n/a	[113]
Aptamer sandwich sensor with Au Np oligomers	thrombin	buffer	10 fM	20 fM–20 nM	n/a	n/a	[114]
Upconversion cross-correlation spectroscopy	thyroid-stimulating hormone	buffer	15 mIU L^{-1}	28.8–2880 mIU L^{-1}	30	30 μL	[102]
Magnetic bead surface coverage assay	TNF-α	serum	60 aM	n/a	20	5 μL	[134]
Single-molecule microarray	tumor suppressor protein p53	buffer	35 fM	100 fM–100 pM	n/a	0.2 nL	[64]

CRP = c-reactive protein; cTnI = cardiac troponin I; AFP = alpha-fetoprotein; FSH = follicle stimulating hormone; hCG = human chorionic gonadotropin; NF-L = neurofilament light chain; TNF-a = tumor necrosis factor alpha.

Table 3: Digital assays for bacteria, viruses, toxins, and other contaminants. The LODs were converted into molar concentrations wherever applicable.

Assay type	Analyte	Matrix	LOD	Working range	Assay time (min)	Sample volume	Ref.
Multiplexed single-virus immunoassay	avian influenza H9N2, H1N1, H7N9	buffer	0.02 pg mL^{-1}	n/a	60	n/a	[131]
Digital MultiPath immunoassay	*C. difficile* toxin B	8% pooled stool sample diluted in buffer	170 fM	100 fM–1 nM	30	100 µL	[133]
Single-QD-based aptamer nanosensor	cocaine	buffer	500 nM	500 nM–10 µM	n/a	n/a	[88]
FCS	fumonisin B_1	buffer	1.4 nM	1.4 nM–35 nM	15	9 µL	[78]
Microfluidic digital HEBA	influenza A nucleoprotein	buffer	4 aM	10 aM–10 pM	10	10 µL	[54]
Bead-based digital ELISA	hepatitis B surface antigens	buffer	139 aM	100 aM–1 pM	210	n/a	[29]
Digital microarray with interferometric detection of plasmonic nanorods	hepatitis B surface antigens	buffer	126 fM	100 fM–100 nM	270	n/a	[128]
Fluorescence coincidence detection	herpes simplex virus	buffer	50 fM	100 fM–100 pM	180	n/a	[79]
Simoa	HIV p24 capsid	human plasma	117 aM	100 aM–100 fM	210	100 µL	[41]
Counting assay with color-coded NPs	respiratory syncytial virus	buffer	20–30 fM	100 fM–100 pM	100	n/a	[87]
Simoa	ricin	buffer	166 aM	100 aM–100 pM	64	n/a	[44]
Single-molecule aptasensor	adenosine, acetamiprid, PCB-77	chicken extract 100× diluted in buffer	300 fM, 350 fM, 720 fM	500 fM–50 pM	n/a	n/a	[66]

H. Balci, Y. Ishitsuka, C. Buranachai, T. Ha, *Annu. Rev. Biochem.* **2008**, *77*, 51 – 76.

[2] a) L. Cohen, D. R. Walt, *Chem. Rev.* **2019**, *119*, 293 – 321; b) P. Holzmeister, G. P. Acuna, D. Grohmann, P. Tinnefeld, *Chem. Soc. Rev.* **2014**, *43*, 1014 – 1028; c) L. Chang, D. M. Rissin, D. R. Fournier, T. Piech, P. P. Patel, D. H. Wilson, D. C. Duffy, *J. Immunol. Methods* **2012**, *378*, 102 – 115; d) J. J. Gooding, K. Gaus, *Angew. Chem. Int. Ed.* **2016**, *55*, 11354 – 11366; *Angew. Chem.* **2016**, *128*, 11526 – 11539; e) Y. F. Wu, R. D. Tilley, J. J. Gooding, *J. Am. Chem. Soc.* **2019**, *141*, 1162 – 1170.

[3] a) R. J. Yu, Y. L. Ying, Y. X. Hu, R. Gao, Y. T. Long, *Anal. Chem.* **2017**, *89*, 8203 – 8206; b) A. Arima, I. H. Harlisa, T. Yoshida, M. Tsutsui, M. Tanaka, K. Yokota, W. Tonomura, J. Yasuda, M. Taniguchi, T. Washio, M. Okochi, T. Kawai, *J. Am. Chem. Soc.* **2018**, *140*, 16834 – 16841.

[4] a) U. Wienken, H. E. Gaub, *Biophys. J.* **2013**, *105*, 2687 – 2694; b) S. Mandal, D. Koirala, S. Selvam, C. Ghimire, H. B. Mao, *Angew. Chem. Int. Ed.* **2015**, *54*, 7607 – 7611; *Angew. Chem.* **2015**, *127*, 7717 – 7721.

[5] S. Subramanian, H. Y. Wu, T. Constant, J. Xavier, F. Vollmer, *Adv. Mater.* **2018**, *30*, 1801246.

[6] I. Surugiu, B. Danielsson, L. Ye, K. Mosbach, K. Haupt, *Anal. Chem.* **2001**, *73*, 487 – 491.

[7] J. Foote, H. N. Eisen, *Proc. Natl. Acad. Sci. USA* **1995**, *92*, 1254 – 1256.

[8] N. M. Green, *Methods Enzymol.* **1990**, *184*, 51 – 67.

[9] R. S. Yalow, S. A. Berson, *Nature* **1959**, *184*, 1648 – 1649.

[10] R. Peltomaa, E. Benito-Pena, M. C. Moreno-Bondi, *Anal. Bioanal. Chem.* **2018**, *410*, 747 – 771.

[11] A. Kunze, L. Pei, D. Elsasser, R. Niessner, M. Seidel, *J. Virol. Methods* **2015**, *222*, 132 – 137.

[12] N. L. Anderson, N. G. Anderson, *Mol. Cell. Proteomics* **2002**, *1*, 845 – 867.

[13] a) S. M. Hanash, S. J. Pitteri, V. M. Faca, *Nature* **2008**, *452*, 571 – 579; b) N. L. Henry, D. F. Hayes, *Mol. Oncol.* **2012**, *6*, 140 – 146; c) M. J. Aernecke, J. Guo, S. Sonkusale, D. R. Walt, *Anal. Chem.* **2009**, *81*, 5281 – 5290; d) D. R. Walt, *J. Clin. Invest.* **2019**, *129*, 3472 – 3473.

[14] J. F. Rusling, C. V. Kumar, J. S. Gutkind, V. Patel, *Analyst* **2010**, *135*, 2496 – 2511.

[15] A. St John, C. P. Price, *Clin. Biochem. Rev.* **2014**, *35*, 155 – 167.

[16] D. J. Litman, T. M. Hanlon, E. F. Ullman, *Anal. Biochem.* **1980**, *106*, 223 – 229.

[17] L. Hood, *Annu. Rev. Anal. Chem.* **2008**, *1*, 1 – 43.

[18] H. Siitari, I. Hemmila, E. Soini, T. Lovgren, V. Koistinen, *Nature* **1983**, *301*, 258 – 260.

[19] M. Rui, C. S. Hampe, C. Wang, Z. D. Ling, F. K. Gorus, A. Lernmark, D. G. Pipeleers, P. E. M. De Pauw, *J. Immunol. Methods* **2007**, *319*, 133 – 143.

[20] a) Z. Farka, T. Juřík, D. Kovář, L. Trnková, P. Skládal, *Chem. Rev.* **2017**, *117*, 9973 – 10042; b) M. Pastucha, Z. Farka, K. Lacina, Z. Mikušová, P. Skládal, *Microchim. Acta* **2019**, *186*, 26.

[21] H. H. Gorris, O. S. Wolfbeis, *Angew. Chem. Int. Ed.* **2013**, *52*, 3584 – 3600; *Angew. Chem.* **2013**, *125*, 3668 – 3686.

[22] a) Z. Farka, M. J. Mickert, A. Hlaváček, P. Skládal, H. H. Gorris, *Anal. Chem.* **2017**, *89*, 11825 – 11830; b) M. J. Mickert, Z. Farka, U. Kostiv, A. Hlaváček, D. Horák, P. Skládal, H. H. Gorris, *Anal. Chem.* **2019**, *91*, 9435 – 9441.

[23] C. Hofmann, A. Duerkop, A. J. Baeumner, *Angew. Chem. Int. Ed.* **2019**, *58*, 12840 – 12860; *Angew. Chem.* **2019**, *131*, 12970 – 12992.

[24] a) A. Shalev, A. H. Greenberg, P. J. Mcalpine, *J. Immunol. Methods* **1980**, *38*, 125 – 139; b) C. C. Harris, R. H. Yolken, H. Krokan, I. C. Hsu, *Proc. Natl. Acad. Sci. USA* **1979**, *76*, 5336 – 5339.

[25] M. Böhmer, J. Enderlein, *ChemPhysChem* **2003**, *4*, 793 – 808.

[26] P. Haas, P. Then, A. Wild, W. Grange, S. Zorman, M. Hegner, M. Calame, U. Aebi, J. Flammer, B. Hecht, *Anal. Chem.* **2010**, *82*, 6299 – 6302.

[27] C. F. Woolley, M. A. Hayes, P. Mahanti, S. D. Gilman, T. Taylor, *Anal. Bioanal. Chem.* **2015**, *407*, 8605 – 8615.

[28] B. Rotman, *Proc. Natl. Acad. Sci. USA* **1961**, *47*, 1981 – 1991.

[29] K. Akama, K. Shirai, S. Suzuki, *Anal. Chem.* **2016**, *88*, 7123 – 7129.

[30] H. H. Gorris, D. R. Walt, *Angew. Chem. Int. Ed.* **2010**, *49*, 3880 – 3895; *Angew. Chem.* **2010**, *122*, 3970 – 3986.

[31] a) R. Liebherr, A. Hutterer, M. Mickert, F. Vogl, A. Beutner, A. Lechner, H. Hummel, H. Gorris, *Anal. Bioanal. Chem.* **2015**, *407*, 7443 – 7452; b) D. M. Rissin, H. H. Gorris, D. R. Walt, *J. Am. Chem. Soc.* **2008**, *130*, 5349 – 5353.

[32] D. B. Craig, E. A. Arriaga, J. C. Y. Wong, H. Lu, N. J. Dovichi, *J. Am. Chem. Soc.* **1996**, *118*, 5245 – 5253.

[33] M. Comellas-Aragonès, H. Engelkamp, V. I. Claessen, N. A. J. M. Sommerdijk, A. E. Rowan, P. C. M. Christianen, J. C. Maan, B. J. M. Verduin, J. J. L. M. Cornelissen, R. J. M. Nolte, *Nat. Nanotechnol.* **2007**, *2*, 635 – 639.

[34] H. M. Piwonski, M. Goomanovsky, D. Bensimon, A. Horovitz, G. Haran, *Proc. Natl. Acad. Sci. USA* **2012**, *109*, E1437 – E1443.

[35] H. Gorris, T. Blicharz, D. Walt, *FEBS J.* **2007**, *274*, 5462 – 5470.

[36] Q. Xue, E. S. Yeung, *Nature* **1995**, *373*, 681 – 683.

[37] Y. Rondelez, G. Tresset, K. V. Tabata, H. Arata, H. Fujita, S. Takeuchi, H. Noji, *Nat. Biotechnol.* **2005**, *23*, 361 – 365.

[38] D. M. Rissin, C. W. Kan, T. G. Campbell, S. C. Howes, D. R. Fournier, L. Song, T. Piech, P. P. Patel, L. Chang, A. J. Rivnak, E. P. Ferrell, J. D. Randall, G. K. Provuncher, D. R. Walt, D. C. Duffy, *Nat. Biotechnol.* **2010**, *28*, 595 – 599.

[39] D. H. Wilson, D. W. Hanlon, G. K. Provuncher, L. Chang, L. N. Song, P. P. Patel, E. P. Ferrell, H. Lepor, A. W. Partin, D. W. Chan, L. J. Sokoll, C. D. Cheli, R. P. Thiel, D. R. Fournier, D. C. Duffy, *Clin. Chem.* **2011**, *57*, 1712 – 1721.

[40] A. D. Warren, S. T. Gaylord, K. C. Ngan, M. D. Milutinovic, G. A. Kwong, S. N. Bhatia, D. R. Walt, *J. Am. Chem. Soc.* **2014**, *136*, 13709 – 13714.

[41] L. Chang, L. N. Song, D. R. Fournier, C. W. Kan, P. P. Patel, E. P. Ferrell, B. A. Pink, K. A. Minnehan, D. W. Hanlon, D. C. Duffy, D. H. Wilson, *J. Virol. Methods* **2013**, *188*, 153 – 160.

[42] P. Shahim, M. Gren, V. Liman, U. Andreasson, N. Norgren, Y. Tegner, N. Mattsson, N. Andreasen, M. Ost, H. Zetterberg, B. Nellgard, K. Blennow, *Sci. Rep.* **2016**, *6*, 36791.

[43] A. Olivera, N. Lejbman, A. Jeromin, L. M. French, H. S. Kim, A. Cashion, V. Mysliwiec, R. Diaz-Arrastia, J. Gill, *JAMA Neurol.* **2015**, *72*, 1109 – 1116.

[44] S. T. Gaylord, T. L. Dinh, E. R. Goldman, G. P. Anderson, K. C. Ngan, D. R. Walt, *Anal. Chem.* **2015**, *87*, 6570 – 6577.

[45] S. H. Kim, S. Iwai, S. Araki, S. Sakakihara, R. Iino, H. Noji, *Lab Chip* **2012**, *12*, 4986 – 4991.

[46] Y. Obayashi, R. Iino, H. Noji, *Analyst* **2015**, *140*, 5065 – 5073.

[47] X. Wang, L. Cohen, J. Wang, D. R. Walt, *J. Am. Chem. Soc.* **2018**, *140*, 18132 – 18139.

[48] M. T. Guo, A. Rotem, J. A. Heyman, D. A. Weitz, *Lab Chip* **2012**, *12*, 2146 – 2155.

[49] H. Song, R. F. Ismagilov, *J. Am. Chem. Soc.* **2003**, *125*, 14613 – 14619.

[50] J. J. Agresti, E. Antipov, A. R. Abate, K. Ahn, A. C. Rowat, J. C. Baret, M. Marquez, A. M. Klibanov, A. D. Griffiths, D. A. Weitz, *Proc. Natl. Acad. Sci. USA* **2010**, *107*, 4004 – 4009.

[51] J. U. Shim, R. T. Ranasinghe, C. A. Smith, S. M. Ibrahim, F. Hollfelder, W. T. S. Huck, D. Klenerman, C. Abell, *ACS Nano* **2013**, *7*, 5955 – 5964.

[52] C. C. Liu, X. N. Xu, B. Li, B. Situ, W. L. Pan, Y. Hu, T. X. An, S. H. Yao, L. Zheng, *Nano Lett.* **2018**, *18*, 4226 – 4232.

[53] S. B. Tian, Z. Zhang, J. Y. Chen, M. Y. Du, Z. Li, H. Yang, X. H. Ji, Z. K. He, *Talanta* **2018**, *186*, 24 – 28.

[54] D. Kim, O. B. Garner, A. Ozcan, D. Di Carlo, *ACS Nano* **2016**, *10*, 7467 – 7475.

[55] D. Schenk, G. Song, Y. Ke, Z. H. Wang, *PLOS One* **2017**, *12*, e0181062.

[56] N. R. Beer, B. J. Hindson, E. K. Wheeler, S. B. Hall, K. A. Rose, I. M. Kennedy, B. W. Colston, *Anal. Chem.* **2007**, *79*, 8471 – 8475.

[57] F. Shen, B. Sun, J. E. Kreutz, E. K. Davydova, W. B. Du, P. L. Reddy, L. J. Joseph, R. F. Ismagilov, *J. Am. Chem. Soc.* **2011**, *133*, 17705 – 17712.

[58] W. H. Zhou, *Anal. Methods* **2018**, *10*, 3690 – 3695.

[59] R. Q. Ke, R. Y. Nong, S. Fredriksson, U. Landegren, M. Nilsson, *Plos One* **2013**, *8*, 5.

[60] B. Oswald, M. Gruber, M. Bohmer, F. Lehman, M. Probst, O. S. Wolfbeis, *Photochem. Photobiol.* **2001**, *74*, 237 – 245.

[61] F. Löscher, S. Böhme, J. Martin, S. Seeger, *Anal. Chem.* **1998**, *70*, 3202 – 3205.

[62] A. Jain, R. J. Liu, B. Ramani, E. Arauz, Y. Ishitsuka, K. Ragunathan, J. Park, J. Chen, Y. K. Xiang, T. Ha, *Nature* **2011**, *473*, 484 – 488.

[63] P. Tinnefeld, *Nature* **2011**, *473*, 461 – 462.

[64] E. Burgin, A. Salehi-Reyhani, M. Barclay, A. Brown, J. Kaplinsky, M. Novakova, M. A. A. Neil, O. Ces, K. R. Willison, D. R. Klug, *Analyst* **2014**, *139*, 3235 – 3244.

[65] H. D. Zhang, Y. J. Liu, K. Zhang, J. Ji, J. W. Liu, B. H. Liu, *Anal. Chem.* **2018**, *90*, 9315 – 9321.

[66] R. Weng, S. T. Lou, L. D. Li, Y. Zhang, J. Qiu, X. Su, Y. Z. Qian, N. G. Walter, *Anal. Chem.* **2019**, *91*, 1424 – 1431.

[67] Y. F. Ma, M. R. Shortreed, H. L. Li, W. H. Huang, E. S. Yeung, *Electrophoresis* **2001**, *22*, 421 – 426.

[68] A. H. B. Wu, N. Fukushima, R. Puskas, J. Todd, P. Goix, *Clin. Chem.* **2006**, *52*, 2157 – 2159.

[69] J. Todd, B. Freese, A. Lu, D. Held, J. Morey, R. Livingston, P. Goix, *Clin. Chem.* **2007**, *53*, 1990 – 1995.

[70] T. J. Esparza, H. Z. Zhao, J. R. Cirrito, N. J. Cairns, R. J. Bateman, D. M. Holtzman, D. L. Brody, *Ann. Neurol.* **2013**, *73*, 104 – 119.

[71] E. J. Wild, R. Boggio, D. Langbehn, N. Robertson, S. Haider, J. R. C. Miller, H. Zetterberg, B. R. Leavitt, R. Kuhn, S. J. Tabrizi, D. Macdonald, A. Weiss, *J. Clin. Invest.* **2015**, *125*, 1979 – 1986.

[72] E. A. Nalefski, C. M. D'Antoni, E. P. Ferrell, J. A. Lloyd, H. Q. Qiu, J. L. Harris, D. H. Whitney, *Clin. Chem.* **2006**, *52*, 2172 – 2175.

[73] S. W. Yim, T. Kim, T. A. Laurence, S. Partono, D. S. Kim, Y. Kim, S. M. Weiss, A. M. Reitmair, *Clin. Chem.* **2012**, *58*, 707 – 716.

[74] Z. Foldes-Papp, U. Demel, G. P. Tilz, *Proc. Natl. Acad. Sci. USA* **2001**, *98*, 11509 – 11514.

[75] S. Y. Tetin, K. M. Swift, E. D. Matayoshi, *Anal. Biochem.* **2002**, *307*, 84 – 91.

[76] M. Chatterjee, B. Noding, E. A. J. Willemse, M. J. A. Koel-Simmelink, W. M. van der Fliere, D. Schild, C. E. Teunissen, *Clin. Biochem.* **2017**, *50*, 1061 – 1066.

[77] S. T. Hess, S. H. Huang, A. A. Heikal, W. W. Webb, *Biochemistry* **2002**, *41*, 697 – 705.

[78] Y. N. Bian, X. Y. Huang, J. C. Ren, *Anal. Methods* **2016**, *8*, 1333 – 1338.

[79] H. T. Li, D. J. Zhou, H. Browne, S. Balasubramanian, D. Klenerman, *Anal. Chem.* **2004**, *76*, 4446 – 4451.

[80] A. E. Miller, C. W. Hollars, S. M. Lane, T. A. Laurence, *Anal. Chem.* **2009**, *81*, 5614 – 5622.

[81] a) A. N. Kapanidis, N. K. Lee, T. A. Laurence, S. Doose, E. Margeat, S. Weiss, *Proc. Natl. Acad. Sci. USA* **2004**, *101*, 8936 – 8941; b) E. Thews, M. Gerken, R. Eckert, J. Zapfel, C. Tietz, J. Wrachtrup, *Biophys. J.* **2005**, *89*, 2069 – 2076.

[82] M. Seydack, *Biosens. Bioelectron.* **2005**, *20*, 2454 – 2469.

[83] E. Petryayeva, W. R. Algar, I. L. Medintz, *Appl. Spectrosc.* **2013**, *67*, 215 – 252.

[84] U. Resch-Genger, M. Grabolle, S. Cavaliere-Jaricot, R. Nitschke, T. Nann, *Nat. Methods* **2008**, *5*, 763 – 775.

[85] X. J. Liu, C. H. Huang, C. H. Zong, A. Y. Liang, Z. J. Wu, Y. S. Zhang, Q. Q. Zhang, W. F. Zhao, H. W. Gai, *ACS Sens.* **2018**, *3*, 2644 – 2650.

[86] X. J. Liu, C. H. Huang, X. L. Dong, A. Y. Liang, Y. S. Zhang, Q. Q. Zhang, Q. Wang, H. W. Gai, *Chem. Commun.* **2018**, *54*, 13103 – 13106.

[87] A. Agrawal, C. Y. Zhang, T. Byassee, R. A. Tripp, S. M. Nie, *Anal. Chem.* **2006**, *78*, 1061 – 1070.

[88] C. Y. Zhang, L. W. Johnson, *Anal. Chem.* **2009**, *81*, 3051 – 3055.

[89] S. R. Jung, R. Han, W. Sun, Y. F. Jiang, B. S. Fujimoto, J. B. Yu, C. T. Kuo, Y. Rong, X. H. Zhou, D. T. Chiu, *Anal. Chem.* **2018**, *90*, 6089 – 6095.

[90] U. Meseth, T. Wohland, R. Rigler, H. Vogel, *Biophys. J.* **1999**, *76*, 1619 – 1631.

[91] J. J. Yin, A. D. Zhang, C. Q. Dong, J. C. Ren, *Talanta* **2015**, *144*, 13 – 19.

[92] L. C. Hwang, T. Wohland, *ChemPhysChem* **2004**, *5*, 549 – 551.

[93] F. Fujii, M. Kinjo, *ChemBioChem* **2007**, *8*, 2199 – 2203.

[94] T. Kogure, S. Karasawa, T. Araki, K. Saito, M. Kinjo, A. Miyawaki, *Nat. Biotechnol.* **2006**, *24*, 577 – 581.

[95] J. J. Wang, H. Liu, X. Y. Huang, J. C. Ren, *Microchim. Acta* **2016**, *183*, 749 – 755.

[96] a) M. Haase, H. Schäfer, *Angew. Chem. Int. Ed.* **2011**, *50*, 5808 – 5829; *Angew. Chem.* **2011**, *123*, 5928 – 5950; b) U. Resch-Genger, H. H. Gorris, *Anal. Bioanal. Chem.* **2017**, *409*, 5855 – 5874; c) H. H. Gorris, U. Resch-Genger, *Anal. Bioanal. Chem.* **2017**, *409*, 5875 – 5890.

[97] Y. Fan, S. F. Wang, F. Zhang, *Angew. Chem. Int. Ed.* **2019**, *58*, 13208 – 13219; *Angew. Chem.* **2019**, *131*, 13342 – 13353.

[98] V. Kale, H. Pakkila, J. Vainio, A. Ahomaa, N. Sirkka, A. Lyytikainen, S. M. Talha, A. Kutsaya, M. Waris, I. Julkunen, T. Soukka, *Anal. Chem.* **2016**, *88*, 4470 – 4477.

[99] L. Zhou, Y. Fan, R. Wang, X. M. Li, L. L. Fan, F. Zhang, *Angew. Chem. Int. Ed.* **2018**, *57*, 12824 – 12829; *Angew. Chem.* **2018**, *130*, 13006 – 13011.

[100] Y. Q. Lu, J. B. Zhao, R. Zhang, Y. J. Liu, D. M. Liu, E. M. Goldys, X. S. Yang, P. Xi, A. Sunna, J. Lu, Y. Shi, R. C. Leif, Y. J. Huo, J. Shen, J. A. Piper, J. P. Robinson, D. Y. Jin, *Nat. Photonics* **2014**, *8*, 33 – 37.

[101] X. Li, L. Wei, L. L. Pan, Z. Y. Yi, X. Wang, Z. J. Ye, L. H. Xiao, H. W. Li, J. F. Wang, *Anal. Chem.* **2018**, *90*, 4807 – 4814.

[102] S. Lahtinen, S. Krause, R. Arppe, T. Soukka, T. Vosch, *Chem. Eur. J.* **2018**, *24*, 9229 – 9233.

[103] W. Becker, in *Springer Ser. Chem. Phys. Bd. 81*, Springer-Verlag, Berlin, Heidelberg, **2005**, S. I-387.

[104] C. Fenzl, T. Hirsch, A. J. Baeumner, *TRAC Trends Anal. Chem.* **2016**, *79*, 306 – 316.

[105] R. Nooney, A. Clifford, X. LeGuevel, O. Stranik, C. McDonagh, B. D. MacCraith, *Anal. Bioanal. Chem.* **2010**, *396*, 1127 – 1134.

[106] C. J. Murphy, A. M. Gole, J. W. Stone, P. N. Sisco, A. M. Alkilany, E. C. Goldsmith, S. C. Baxter, *Acc. Chem. Res.* **2008**, *41*, 1721 – 1730.

[107] C. Y. Poon, L. Wei, Y. L. Xu, B. Chen, L. H. Xiao, H. W. Li, *Anal. Chem.* **2016**, *88*, 8849 – 8856.

[108] X. Wu, T. Li, G. Y. Tao, R. Y. Lin, X. J. Pei, F. Liu, N. Li, *Analyst* **2017**, *142*, 4201 – 4205.

[109] L. Zhu, G. H. Li, S. Q. Sun, H. Tan, Y. H. He, *RSC Adv.* **2017**, *7*, 27595 – 27602.

[110] M. Sriram, B. P. Markhali, P. R. Nicovich, D. T. Bennett, P. J. Reece, D. B. Hibbert, R. D. Tilley, K. Gaus, S. R. C. Vivekchand, J. J. Gooding, *Biosens. Bioelectron.* **2018**, *117*, 530 – 536.

[111] E. Lüthgens, A. Janshoff, *ChemPhysChem* **2005**, *6*, 444 – 448.

[112] S. S. Aćimović, H. Šípová-Jungová, G. Emilsson, L. Shao, A. B. Dahlin, M. Käll, T. J. Antosiewicz, *ACS Nano* **2018**, *12*, 9958 – 9965.

[113] R. Yang, S. W. Liu, Z. J. Wu, Y. Tan, S. Q. Sun, *Talanta* **2018**, *182*, 348 – 353.

[114] J. J. Li, Y. F. Jiao, Q. Y. Liu, Z. B. Chen, *Anal. Chim. Acta* **2018**, *1028*, 66 – 76.

[115] S. Chen, M. Svedendahl, R. P. Van Duyne, M. Kall, *Nano Lett.* **2011**, *11*, 1826 – 1830.

[116] X. Liu, Q. Dai, L. Austin, J. Coutts, G. Knowles, J. H. Zou, H. Chen, Q. Huo, *J. Am. Chem. Soc.* **2008**, *130*, 2780 – 2782.

[117] T. Lan, C. A. Dong, X. Y. Huang, J. C. Ren, *Analyst* **2011**, *136*, 4247 – 4253.

[118] T. Lan, C. Q. Dong, X. Y. Huang, J. C. Ren, *Talanta* **2013**, *116*, 501 – 507.

[119] J. J. Wang, X. Y. Huang, H. Liu, C. Q. Dong, J. C. Ren, *Anal. Chem.* **2017**, *89*, 5230 – 5237.

[120] B. Rothenhäusler, W. Knoll, *Nature* **1988**, *332*, 615 – 617.

[121] I. Sidorenko, S. Nizamov, R. Hergenroder, A. Zybin, A. Kuzmichev, B. Kiwull, R. Niessner, V. M. Mirsky, *Microchim. Acta* **2016**, *183*, 101 – 109.

[122] B. Huang, F. Yu, R. N. Zare, *Anal. Chem.* **2007**, *79*, 2979 – 2983.

[123] A. Zybin, Y. A. Kuritsyn, E. L. Gurevich, V. V. Temchura, K. Uberla, K. Niemax, *Plasmonics* **2010**, *5*, 31 – 35.

[124] J. Homola, *Chem. Rev.* **2008**, *108*, 462 – 493.

[125] S. Nizamov, V. Scherbahn, V. M. Mirsky, *Anal. Chem.* **2016**, *88*, 10206 – 10214.

[126] S. Nizamov, O. Kasian, V. M. Mirsky, *Angew. Chem. Int. Ed.* **2016**, *55*, 7247 – 7251; *Angew. Chem.* **2016**, *128*, 7363 – 7367.

[127] A. R. Halpern, J. B. Wood, Y. Wang, R. M. Corn, *ACS Nano* **2014**, *8*, 1022 – 1030.

[128] D. Sevenler, G. G. Daaboul, F. E. Kanik, N. L. Unlu, M. S. Unlu, *ACS Nano* **2018**, *12*, 5880 – 5887.

[129] A. Belushkin, F. Yesilkoy, H. Altug, *ACS Nano* **2018**, *12*, 4453 – 4461.

[130] H. Härmä, T. Soukka, T. Lövgren, *Clin. Chem.* **2001**, *47*, 561 – 568.

[131] Z. Wu, T. Zeng, W. J. Guo, Y. Y. Bai, D. W. Pang, Z. L. Zhang, *ACS Appl. Mater. Interfaces* **2019**, *11*, 5762 – 5770.

[132] F. Zhang, Q. H. Shi, Y. C. Zhang, Y. F. Shi, K. L. Ding, D. Y. Zhao, G. D. Stucky, *Adv. Mater.* **2011**, *23*, 3775 – 3779.

[133] S. Gite, D. Archambault, M. P. Cappillino, D. Cunha, V. Dorich, T. Shatova, A. Tempesta, B. Walsh, J. A. Walsh, A. Williams, J. E. Kirby, J. Bowers, D. Straus, *Sci. Rep.* **2018**, *8*, 8.
[134] H. C. Tekin, M. Cornaglia, M. A. M. Gijs, *Lab Chip* **2013**, *13*, 1053 – 1059.
[135] D. A. Schafer, J. Gelles, M. P. Sheetz, R. Landick, *Nature* **1991**, *352*, 444 – 448.
[136] E. W. A. Visser, J. H. Yan, L. J. van Ijzendoorn, M. W. J. Prins, *Nat. Commun.* **2018**, *9*, 2541.
[137] J. Silver, Z. Y. Li, K. Neuman, *Biosens. Bioelectron.* **2015**, *63*, 117 – 123.
[138] K. Akama, N. Iwanaga, K. Yamawaki, M. Okuda, K. Jain, H. Ueno, N. Soga, Y. Minagawa, H. Noji, *ACS Nano* **2019**, *13*, 13116 – 13126.
[139] A. B. Taylor, P. Zijlstra, *ACS Sens.* **2017**, *2*, 1103 – 1122.
[140] B. Sepúlveda, P. C. Angelomé, L. M. Lechuga, L. M. Liz-Marzán, *Nano Today* **2009**, *4*, 244 – 251.
[141] N. J. Halas, S. Lal, W. S. Chang, S. Link, P. Nordlander, *Chem. Rev.* **2011**, *111*, 3913 – 3961.
[142] M. A. Beuwer, B. van Hoof, P. Zijlstra, *J. Phys. Chem. C* **2018**, *122*, 4615 – 4621.
[143] M. Garai, T. S. Zhang, N. Y. Gao, H. Zhu, Q. H. Xu, *J. Phys. Chem. C* **2016**, *120*, 11621 – 11630.
[144] A. Kinkhabwala, Z. F. Yu, S. H. Fan, Y. Avlasevich, K. Mullen, W. E. Moerner, *Nat. Photonics* **2009**, *3*, 654 – 657.
[145] P. Zijlstra, P. M. R. Paulo, K. Yu, Q. H. Xu, M. Orrit, *Angew. Chem. Int. Ed.* **2012**, *51*, 8352 – 8355; *Angew. Chem.* **2012**, *124*, 8477 – 8480.
[146] S. E. Lee, Q. Chen, R. Bhat, S. Petkiewicz, J. M. Smith, V. E. Ferry, A. L. Correia, A. P. Alivisatos, M. J. Bissell, *Nano Lett.* **2015**, *15*, 4564 – 4570.
[147] M. A. Beuwer, M. W. J. Prins, P. Zijlstra, *Nano Lett.* **2015**, *15*, 3507 – 3511.
[148] A. L. Washburn, M. S. Luchansky, A. L. Bowman, R. C. Bailey, *Anal. Chem.* **2010**, *82*, 69 – 72.
[149] M. D. Baaske, F. Vollmer, *Nat. Photonics* **2016**, *10*, 733 – 739.
[150] M. F. S. Ferreira, E. Castro-Camus, D. J. Ottaway, J. M. Lopez-Higuera, X. Feng, W. Jin, Y. Jeong, N. Picque, L. M. Tong, B. M. Reinhard, P. M. Pellegrino, A. Mendez, M. Diem, F. Vollmer, Q. M. Quan, *J. Optics* **2017**, *19*, 083001.
[151] A. B. Zrimsek, N. H. Chiang, M. Mattei, S. Zaleski, M. O. McAnally, C. T. Chapman, A. I. Henry, G. C. Schatz, R. P. Van Duyne, *Chem. Rev.* **2017**, *117*, 7583 – 7613.
[152] Single Molecule Counting (SMC) Erenna Instrument, Software and Kits http://www.merckmillipore.com/CZ/cs/life-science-research/protein-detection-quantification/Immunoassay-Platform-Solutions/single-molecule-counting-immunoassay-technology/SMC-Erenna-Instrument-Software-and-Kits/VS.b.qB.N.UAAAFfn7lc20.J,nav.
[153] Simoa assay kits https://www.quanterix.com/products-technology/simoa-assay-kits.
[154] L. Smith, M. Kohli, A. M. Smith, *J. Am. Chem. Soc.* **2018**, *140*, 13904 – 13912.
[155] D. Yeung, S. Ciotti, S. Purushothama, E. Gharakhani, G. Kuesters, B. Schlain, C. Shen, D. Donaldson, A. Mikulskis, *J. Immunol. Methods* **2016**, *437*, 53 – 63.
[156] O. R. Costa, K. Verhaeghen, S. Roels, G. Starige, Z. D. Ling, D. Pipeleers, F. K. Gorus, G. A. Martens, *PLOS One* **2018**, *13*, e0193670.

Manuscript received: October 31, 2019
Revised manuscript received: December 20, 2019
Accepted manuscript online: December 23, 2019
Version of record online: April 15, 2020

